Chapter 2: LITERATURE REVIEW AND BACKGROUND

2.1 Whitetopping Overlay

Three types of whitetoppings are common in practice, (i) conventional whitetopping, slab thickness (h_{PCC}) > 6 in; (ii) thin whitetopping (TWT), h_{PCC} = 4 to 6 in and (iii) ultra-thin whitetopping (UTW), $h_{PCC} \leq 4$ in. In ultra-thin whitetopping, bonding between the concrete overlay and the underlying HMA layer is ensured for the desired performance. This allows for a thinner concrete overlay, while still fulfilling the intended service life. The bonding between the layers ensures that the two layers act like a single composite layer. This eventually reduces the tensile stress in the overlay, as shown in the schematic in Figure 2-1.

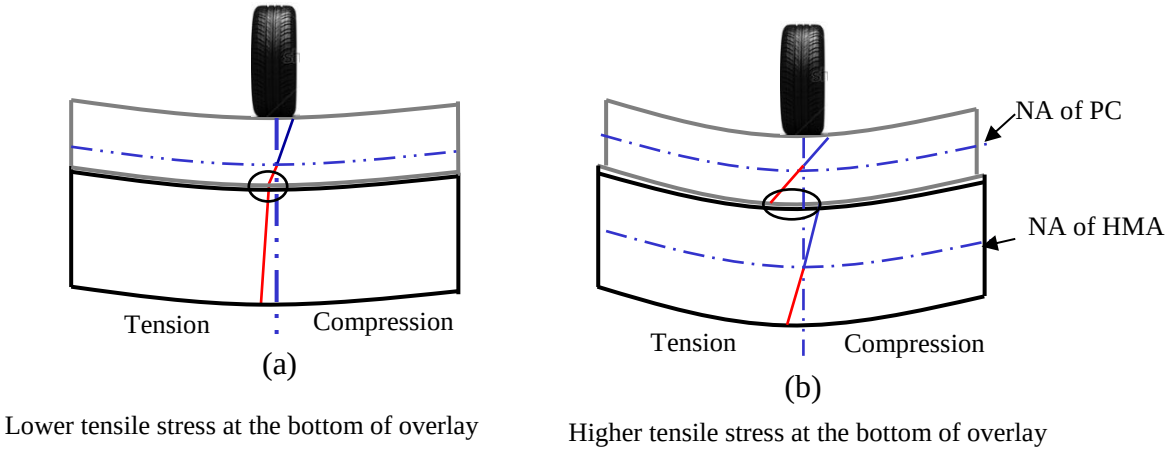

Figure 2-1: Stress distribution through the layers: (a) bonded and (b) unbonded whitetoppings.

2.2 Whitetopping Overlay

Whitetopping as a rehabilitation method was reported in the literature as early as 1918, though a very few projects were noted until the 1990s (Rasmussen & Rozycki, 2004). Since 1992, this rehabilitation method has gained momentum in the United States. Several other countries, such as Canada, Chile, Brazil and Taiwan have also constructed whitetopping overlays (Roesler, et al., 2008).

The increasing popularity of whitetopping has triggered many agencies to put effort towards the development of design procedures. Many agencies, namely the Portland Cement Association

(PCA) (Wu, et al., 1998), the Colorado Department of Transportation (CDOT) (Tarr, et al., 1998; Sheehan, et al., 2004), the New Jersey Department of Transportation (NJDOT) (Gucunski, 1998), the American Concrete Pavement Association (ACPA) (ACPA, 1998 and Riley, et al., 2005), Illinois Center for Transportation (ICT) (Roesler, et al., 2008) and BCOA-ME developed at the University of Pittsburgh (Barman, et al., 2010, Mu & Vandenbossche, 2010, Barman, et al., 2011) have proposed their own design procedures. Each procedure has its own merits and demerits in comparison to the others and addresses a specific whitetopping type, with the exception of the BCOA-ME procedure which allows the design of both thin and ultra-thin overlays. The NCHRP Synthesis 338 (Rasmussen & Rozycki, 2004) indicates that the Arizona, Iowa, Illinois, Mississippi, Texas, Missouri, Kansas and Utah departments of transportation (DOT) adopted the ACPA design procedure, which was actually developed for UTW. Some states, including Colorado, use the CDOT design procedure, mainly developed for TWT. While others attempted to apply the 1993 American Association of State Highway Transportation Officials (AASHTO) Guide for the Design of Pavement Structures, which was actually not intended for the design of thin or ultra-thin whitetopping. The most recent whitetopping design procedure, BCOA-ME, which was developed at the University of Pittsburgh, was jointly funded by many states such as Pennsylvania, Minnesota, Texas, Missouri, New Jersey, Mississippi, Iowa, North Carolina, Kansas and South Dakota. The main advantage of this procedure over the other available procedures is the climatic consideration.

In all the procedures, the basic design approach is same. The design input such as traffic, design life, concrete and existing HMA layer thicknesses, slab size, concrete and HMA layer material properties, base/subbase material properties are considered in the structural response model to estimate the critical stress and strain. Then, the estimated stress and strain are used in the fatigue damage prediction models to predict the fatigue accumulation over the design period. Multiple iterations are performed to select the design thickness. The thickness, which approximates 100% fatigue damage over the design period, is selected as the design thickness. The one disadvantage of these procedures is that the effect of joint performance in determining the critical stress is not addressed. Since, the joint performance has an influence on the potential for debonding; consideration of the joint performance in the design procedure should influence the design life.

2.3 Bonded Whitetopping Failure Modes

The distress types in bonded whitetopping are primarily functions of the slab size and slab thickness, while the deterioration rate appears to be more related to the joint performance, HMA layer thickness, HMA materials stiffness, traffic, climate and more importantly the joint layout. When the longitudinal joints coincide with the wheel path, the distresses progress more rapidly.

The PCA (Wu, et al., 1998) and the ICT whitetopping design procedures (Roesler, et al., 2008) consider corner crack as the primary failure mode for UTW. The CDOT design procedure (Tarr, et al., 1998; Sheehan, et al., 2004) considers transverse crack as the primary mode of failure for thin TWT. A review of the performance of bonded whitetopping performed at the University of Pittsburgh (Barman, et al., 2010) examined the failure modes for bonded whitetopping projects constructed throughout the United States. It was found that the primary mode of distress for the overlays with shorter slab size like 3 ft x 3 ft or 4 ft x 4 ft is corner cracking. Larger slab sizes, like 6 ft x 6 ft and 5 ft x 6 ft, exhibited longitudinal cracks. Examples of these two types of cracks, observed in Minnesota Road Research Project (MnROAD) whitetopping sections, can be seen in Figure 2-2. MnROAD is a full-scale pavement test facility consisting of a 3.5-mile section of interstate (I-94) and a 2.5-mile low-volume roadway near Albertville, Minnesota, approximately 35 miles northwest of Minneapolis. This research facility constructed with many whitetopping test sections with different design features, along with other types of pavements.

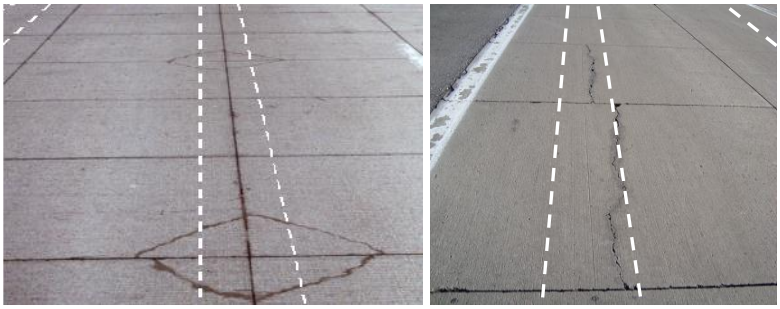

(a) (b) (c)

Figure 2-2: Common failure modes in whitetopping: (a) Corner crack in shorter slabs, (b) Longitudinal crack in larger slabs and (c) Reflected transverse crack (Vandenbossche, 2003, Burnham, 2006 and Barman, et al., 2010).

The in-depth analysis of the distress data of MnROAD whitetopping cells further indicated that most of the transverse cracks were not load related; typically, they are either reflection cracks or secondary cracks that developed off from the already initiated corner cracks (Vandenbossche & Barman, 2010). In Figure 2-2 (c), one such transverse crack is shown. It can be seen that this transverse crack is continued through the HMA shoulder. Pre overlay distress surveys revealed that the HMA layer underneath the whitetopping already had a crack, at this location

Therefore, it can be concluded that in 6-ft x 6-ft slabs when the wheel path is away from the longitudinal joint, longitudinal cracks or diagonal cracks that initiate like longitudinal cracks but then propagate towards the longitudinal joint develop. In shorter slabs, when the longitudinal joint lies at or near the wheel path, corner cracks are the primary mode of distress.

The analysis of the distress data from the MnROAD projects also provides some hints regarding the locations of the crack initiation. In the larger slabs, longitudinal cracks generally initiate at the transverse joint in the wheel path. In the shorter slabs, it is difficult to conclude whether the cracks initiate at the longitudinal edge or at the transverse edge of the slab. When the joint condition deteriorates, the presence of moisture coupled with higher deflections on both the slabs creates debonding of the HMA layer. This results in a higher stress at the loaded slab.

2.4 Joint Performance Terminologies

Distress in bonded whitetopping tends to initiate at or near the joints. In other words, the long term performance of bonded whitetopping depends on the joint performance. Since the present project focuses on the joint performance aspect, it has been thought to provide an introduction of the different parameters which are conventionally used to characterize the joint performance.

***Load transfer efficiency (LTE)*:** The deflection load transfer efficiency, or simply load transfer efficiency (LTE) in this dissertation, is defined as the ratio of the deflections on the unloaded slab to the deflection on the loaded slab, as given below, Equation (2-1).

$$LTE = \frac{\delta_U}{\delta_L} \times 100 \text{ percent} \quad \textbf{(2-1)}$$

where δ_U and δ_L are the deflections on the unloaded and on the loaded side of a joint, respectively. A schematic of a loaded concrete pavement joint explaining the poor and good

joint performance is shown in Figure 2-3. At poor or no joint performance, no load is transferred to the unloaded side, therefore, deflection at the unloaded side is zero ($\delta_U = 0$). In this case, LTE is obtained as 0%. At good load transfer, the deflection at the unloaded side is not zero, and the deflections at both the sides are equal ($\delta_L = \delta_U$); when LTE is obtained as 100%.

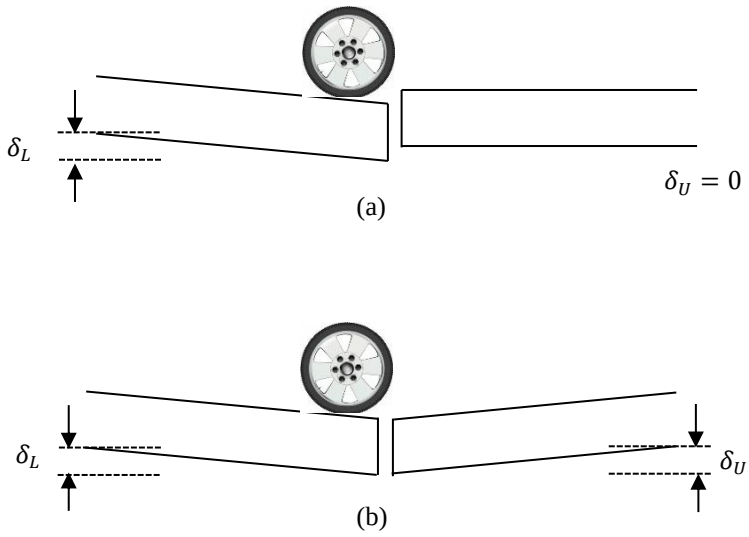

δ_L= Deflection under the loaded slab; δ_U= Deflection under the unloaded slab

Figure 2-3: Joint performance demonstration (a) Poor joint performance (LTE = 0%), (b) Good joint performance (LTE = 100%).

***Joint stiffness (AGG) and non-dimensional joint stiffness (AGG*)*:** Ioannides & Korovesis, 1990 characterized the joint performance of conventional concrete pavement in terms of the aggregate interlock shear stiffness, commonly known as *AGG*. The higher the shear stiffness, the higher the joint performance. They proposed a relationship between the non-dimensional joint stiffness (*AGG**), given in Equation (2-2), and LTE. The mathematical relationship can be seen in Equation (2-3).

$$AGG^* = AGG/kl \tag{2-2}$$

$$LTE = \frac{1}{1+\log^{-1}\left[\frac{0.214-0.183\left(\frac{r}{l}\right)-\log\left(\frac{AGG}{kl}\right)}{1.180}\right]} \tag{2-3}$$

where *r* is the radius of the loaded area, *k* is the modulus of subgrade reaction and *l* is the radius of relative stiffness, which can be obtained by using the following equation.

$$l = \left(\frac{Eh^3}{12(1-\mu^2)k}\right)^{\frac{1}{4}} \quad \textbf{(2-4)}$$

where E and μ are the modulus of elasticity and Poisson's ratio of the concrete, h is the thickness of the concrete slab and k is the modulus of subgrade reaction. The graphical relationship between the LTE and *AGG** is presented in Figure 2-4. It can be seen that the relationship between the LTE and *AGG** can be explained by a sigmoidal function. The relation is linear when the LTE is in between 20 to 80%. Outside this range *AGG** is highly sensitive to LTE.

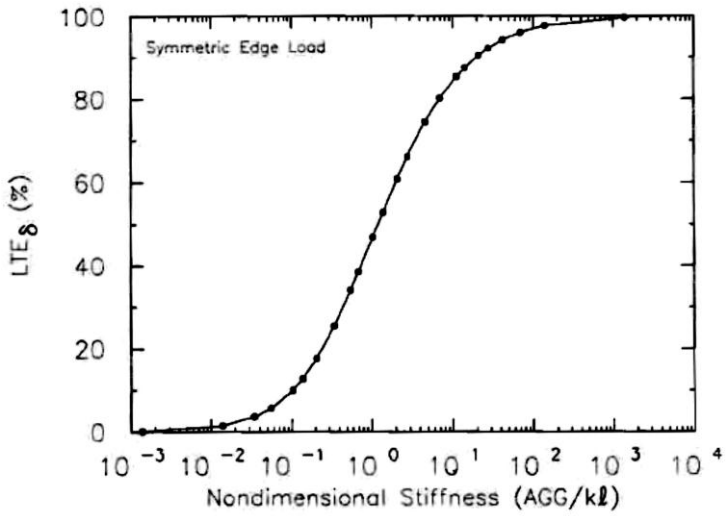

Figure 2-4: Relation between non-dimensional joint stiffness (*AGG) and LTE (Ioannides & Korovesis, 1990).**

Differential deflection (DD): The differential deflection (DD) is defined as the difference between the deflections on the loaded slab and the unloaded slab, as given below, Equation (2-5).

$$DD = \delta_L - \delta_U \quad \textbf{(2-5)}$$

At a higher joint performance, the differential deflection is low, and it becomes zero when LTE is 100%.

Differential energy dissipation (DED): Differential energy dissipation (DED) is derived from the load vs deflection graph. When the pavement system deflects under the wheel load, energy is dissipated out of the system. The magnitude of the dissipated energy (DE) is proportional to the magnitude of the pavement deflection. The dissipated energy is defined as the area under the load vs deflection curve. In a concrete pavement, the magnitude of DE at the approach side

differs from the leave side, based on the joint performance. This difference is referred as the differential energy dissipation (DED) in this dissertation. The ratio between the DE of unloaded and loaded sides is referred as the dissipated energy ratio (DER)

2.5 Joint Performance Medium

In bonded whitetopping, the overlay remains bonded with the HMA layer. The HMA layer is mostly a continuous layer underneath the overlay. Because of all these reasons, a larger portion of the wheel load may be transferred through HMA layer. However, many researchers (Nishizawa, et al., 2003 and Roesler & Wang, 2009) believe that the thin concrete overlay also transfers some amount of load. To determine which layer actually transfers a larger portion of the load, joint performance data from the MnROAD whitetopping sections were studied. The design features of three of the MnROAD whitetopping cells, namely Cell 94, 95 and 96 are given in Table 2-1. All of these three cells were constructed on a thick HMA layer. Joint performance data for these three consecutive years (1998 to 2000) are shown in Figure 2-5 through Figure 2-7. The variation in LTE with temperature for Cell 94 (4-ft x 4-ft slab, 3-in thick overlay on 10-in HMA layer) and Cell 96 (5-ft x 6-ft slab, 6-in thick overlay on 7-in HMA layer) reveals that LTE did increase with the increase in temperature.

Table 2-1: Summary of the design features for Cells 94, 95 and 95 in MnROAD (Barman, et al., 2010).

Cell No.	Age	Thickness of PCC slab (in)	Thickness of HMA layer (in)	Size of the slab (ft × ft)	Sealed joint (Y/N)	Doweled joint (Size/N)	Type of fiber reinforcement
94	Oct 97- Oct 04	3	10	4 × 4	Y	N	Polypropylene
95	Oct 97- Oct 04	3	10	5 x 6	Y	N	Polyolefin
96	Oct 97- current	6	7	5 x 6	Y	N	Polypropylene

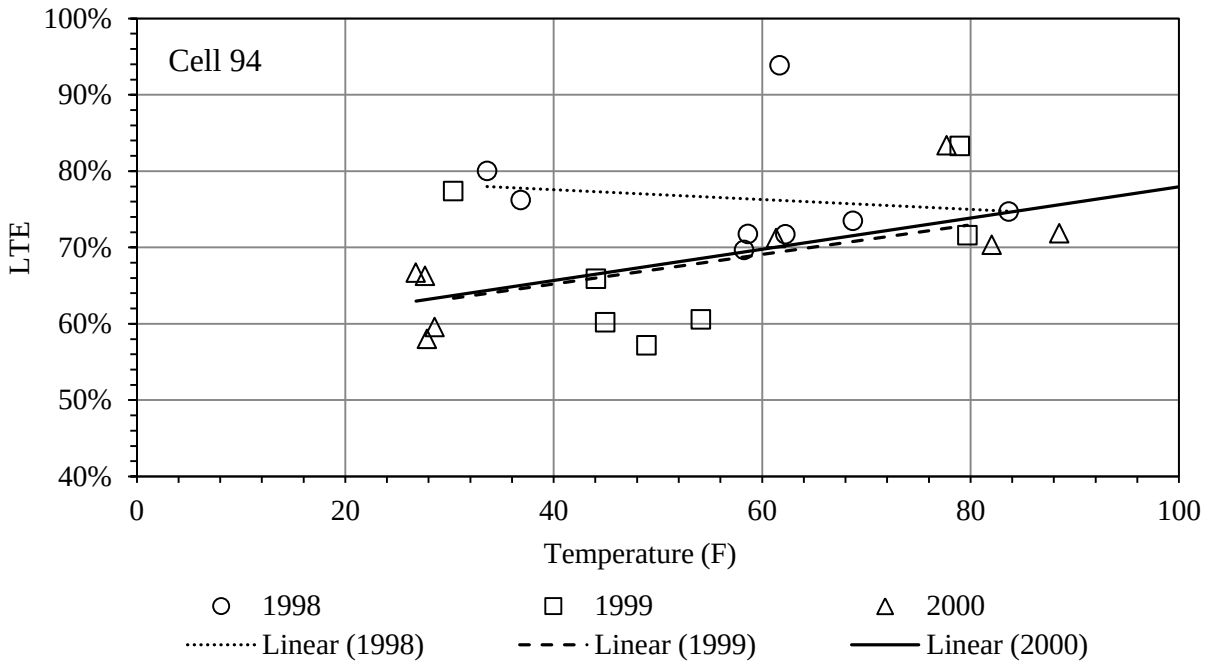

Figure 2-5: LTE vs pavement surface temperature for MnROAD Cell 94.

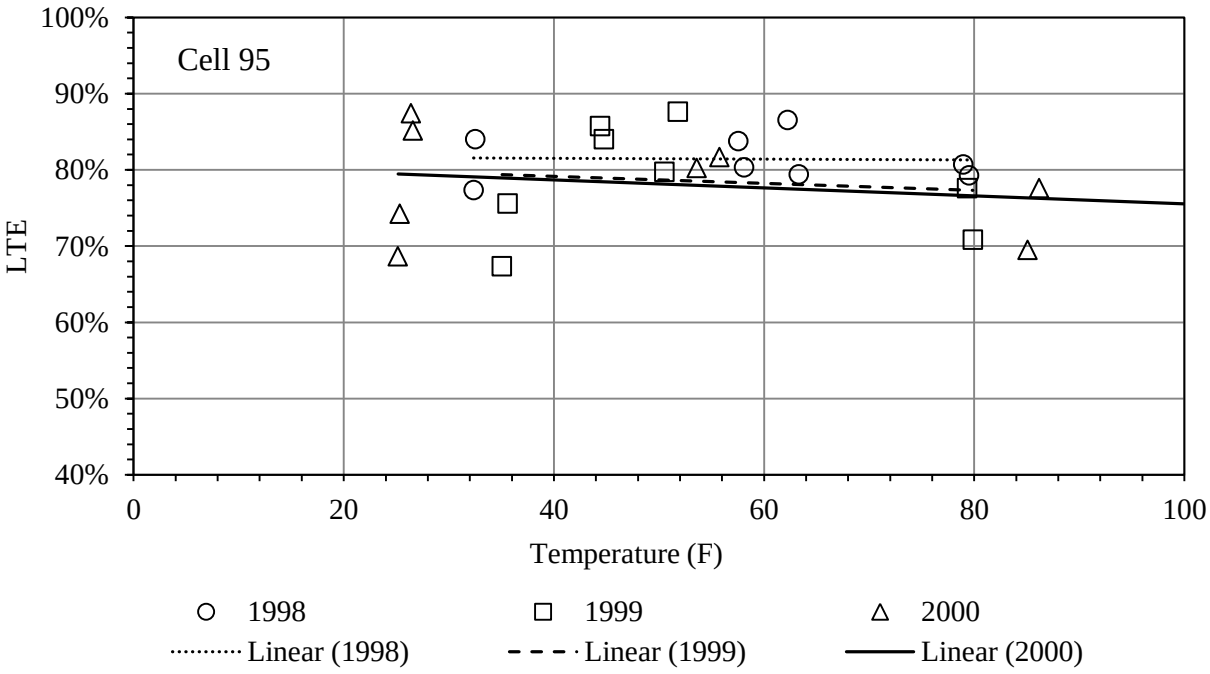

Figure 2-6: LTE vs pavement surface temperature for MnROAD Cell 95.

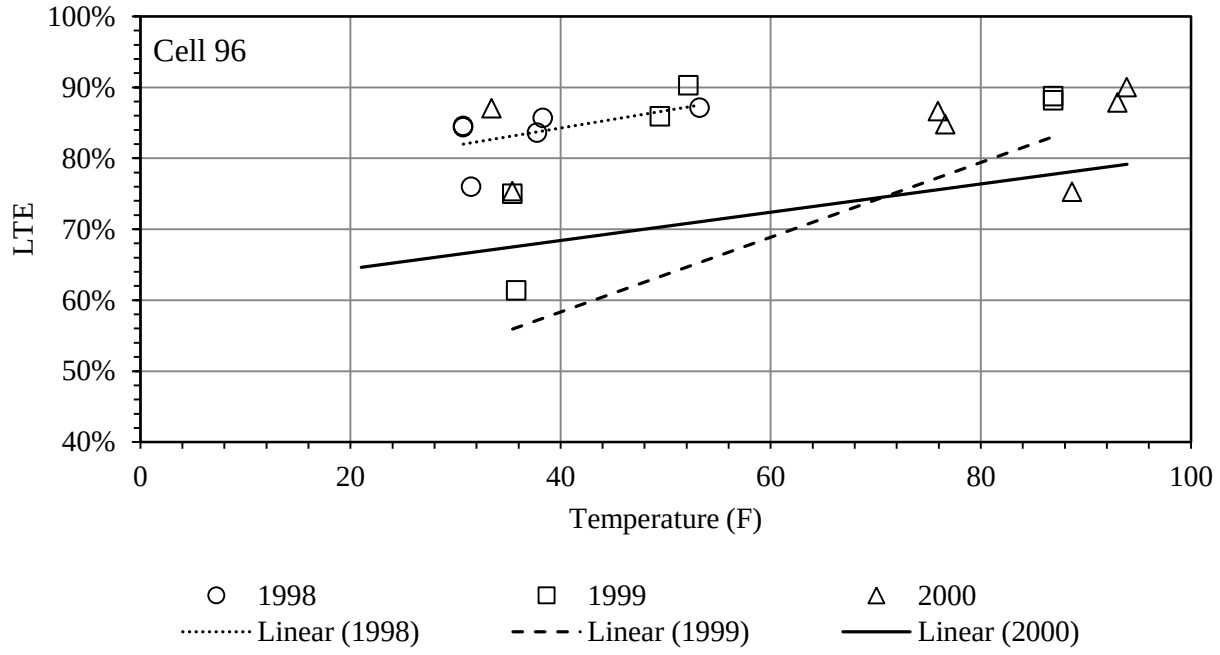

Figure 2-7: LTE vs pavement surface temperature for MnROAD Cell 96.

The LTE for Cell 95, which is a 5-ft x 6-ft slab and 3-in thick overlay on a 10-in HMA layer shows that LTE did not increase with temperature, rather dropped by a marginal amount. Generally, when LTE is contributed through the aggregate interlock, LTE should increase with an increase in the temperature because of a narrower crack width at a higher temperature. Since the LTE increased with the temperature in Cells 94 and 96, it can be concluded that a good amount of load was also being transferred through the concrete slabs. The opposite trend of the LTE vs temperature in Cell 95 can be explained by the fact that the loss of load transfer through HMA layer was larger than the increase in load transfer through the aggregate interlock in an increased temperature in summer. Moreover, Cell 95 was constructed with structural synthetic fibers, which might have helped in transferring load across the concrete slabs. LTE therefore always remained high for this cell, irrespective of the temperature variation. Therefore, it may be stated that when the HMA layer is thick, both the PC and HMA layers transfer load.

Roesler, et al., 2008 performed a study on the joint performance characteristics of the UTW constructed on a thin HMA layer. In that study, the frequencies of cracked joints were recorded. In a 4-ft x 4-ft UTW project constructed over a parking lot at the University of Illinois at Urbana-Champaign (UIUC) campus during Summer 2006, it was observed that every 5th to 8th joint

cracked after approximately 24 hours. This UTW project was built with a 3.5- in FRC on a very thin, approximately 2-in HMA layer. FWD and ultrasonic testing was performed to evaluate joint load transfer after construction (in August 2006) and again after a couple of months (in October 2006). Figure 2-8 and Figure 2-9 present the LTEs measured at different stations in August 2006 and October 2006, respectively. In Figure 2-8, it can be seen that every 5th to 8th joints resulted in a lower LTE. A considerably low LTE at the joints as compared to the LTE at center locations is an indication of the joints that cracked. Station numbers 5, 10 and 17 are assumed to have cracked 24 hours after construction. In Figure 2-9, it can be seen that two months after construction, almost every other joint cracked. The other observation from the two figures is that the joints which cracked 24-hours after construction exhibited a lower LTE. Because of the longer effective length of the slab, the crack width became wider and a lower LTE was obtained as a result. This study indicates that when both the HMA and PC layers are very thin, almost every other joint crack and both the layers have influence on the joint performance.

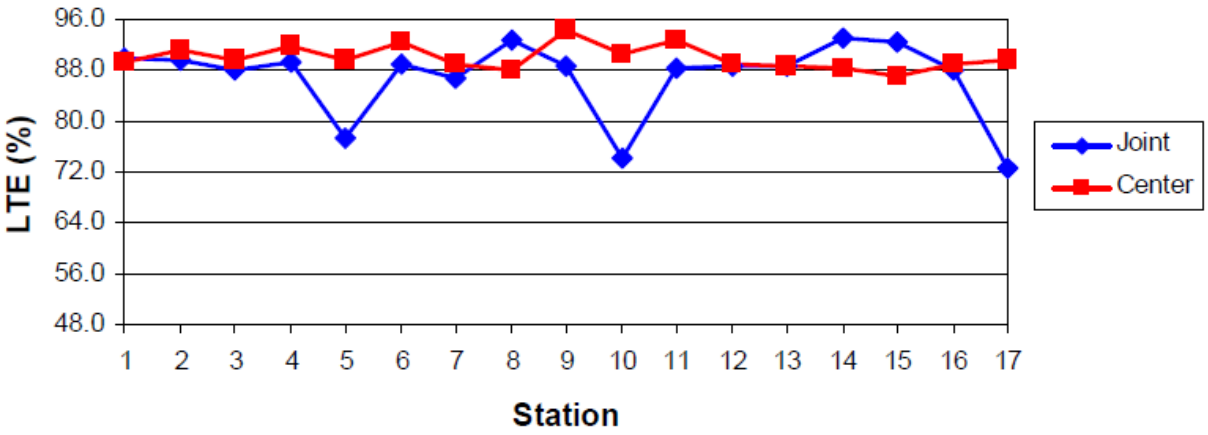

Figure 2-8: Load transfer efficiencies for UIUC E-15 Parking Lot – Parking Bay 1 (August 2006).

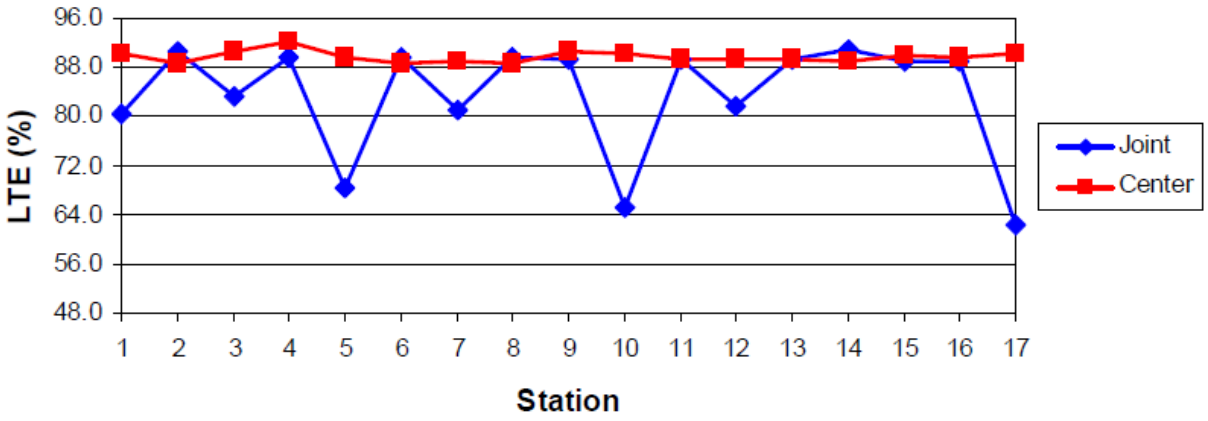

Figure 2-9: Load transfer efficiencies for UIUC E-15 Parking Lot – Parking Bay 1 (October 2006).

2.6 Joint Crack Width Ranges

In another study, Roesler & Wang, 2009 pointed out that since small size slabs are used in whitetopping, the joint opening remains narrow. Crack width data from MnROAD whitetopping sections were studied to establish possible crack width range in different seasons. Figure 2-10 through Figure 2-12 present the crack widths for a few successive joints for Cells 93, 94 and 95, respectively, measured on different dates. The design features of Cells 94 and 95 were presented in Table 2-1and the same information for Cell 93 is presented in Table 2-2. In Figure 2-10 (Cell 93), it can be seen that atleast one of the six joints actually cracked. The crack width varies with season. Also, crack width variation is not the same for all the joints. The maximum crack width (~ 0.030 in) was observed for Joint number 3, in April 1998. In Figure 2-11 (Cell 94), it can be seen that every other joint exhibited a wider crack width. Joints 2 and 4 had the widest crack width, with the maximum occurring during the winter months (~ 0.042 to 0.068 in). In Figure 2-12 (Cell 95), Joints 2 and 5 exhibited wider crack widths, and again the widest crack width was observed during the winter months (~ 0.035 to 0.070 in).

Table 2-2: Summary of the design features for Cell 93 at MnROAD (Barman, et al., 2010).

Cell No.	Age	Thickness of PCC slab (in)	Thickness of HMA layer (in)	Size of the slab (ft × ft)	Sealed joint (Y/N)	Doweled joint (Size/N)	Type of fiber reinforcement
93	Oct 97-Oct 04	4	9	4 × 4	Y	N	Polypropylene

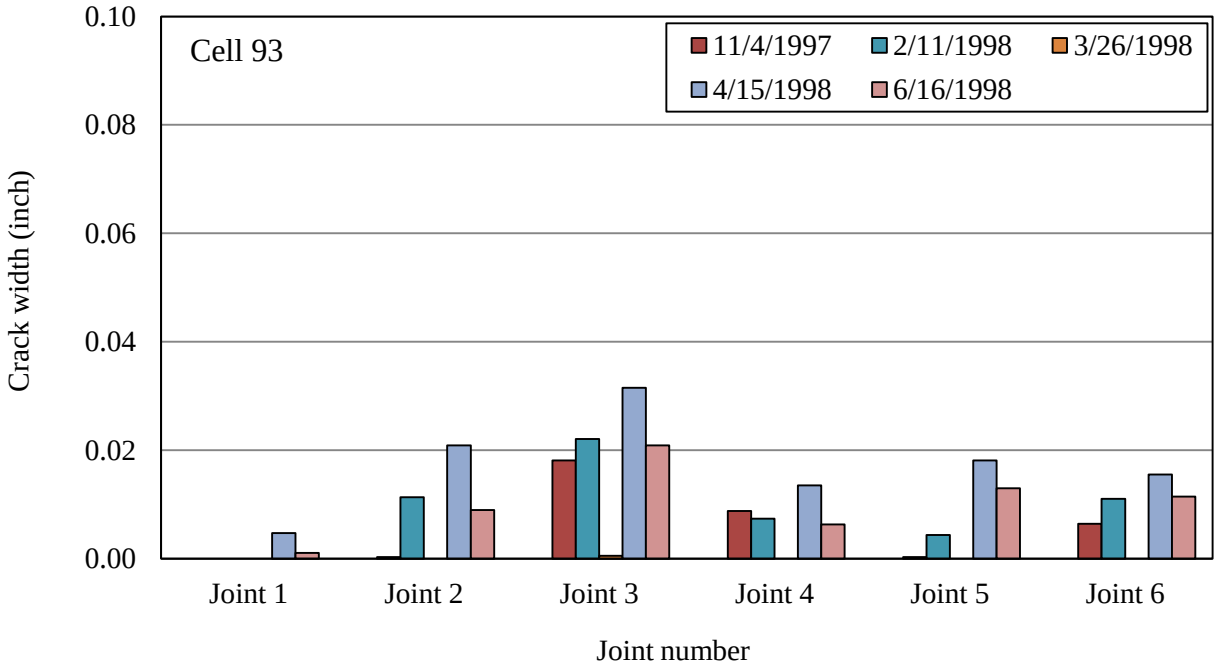

Figure 2-10: Crack width at different joints for MnROAD Cell 93.

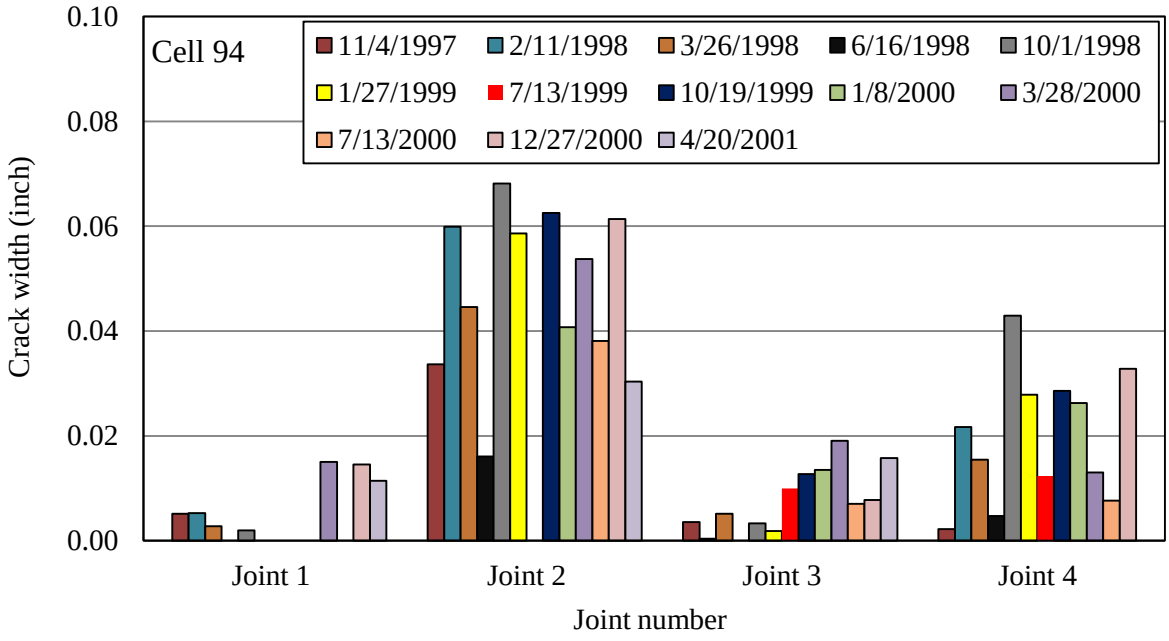

Figure 2-11: Crack width at different joints for MnROAD Cell 94.

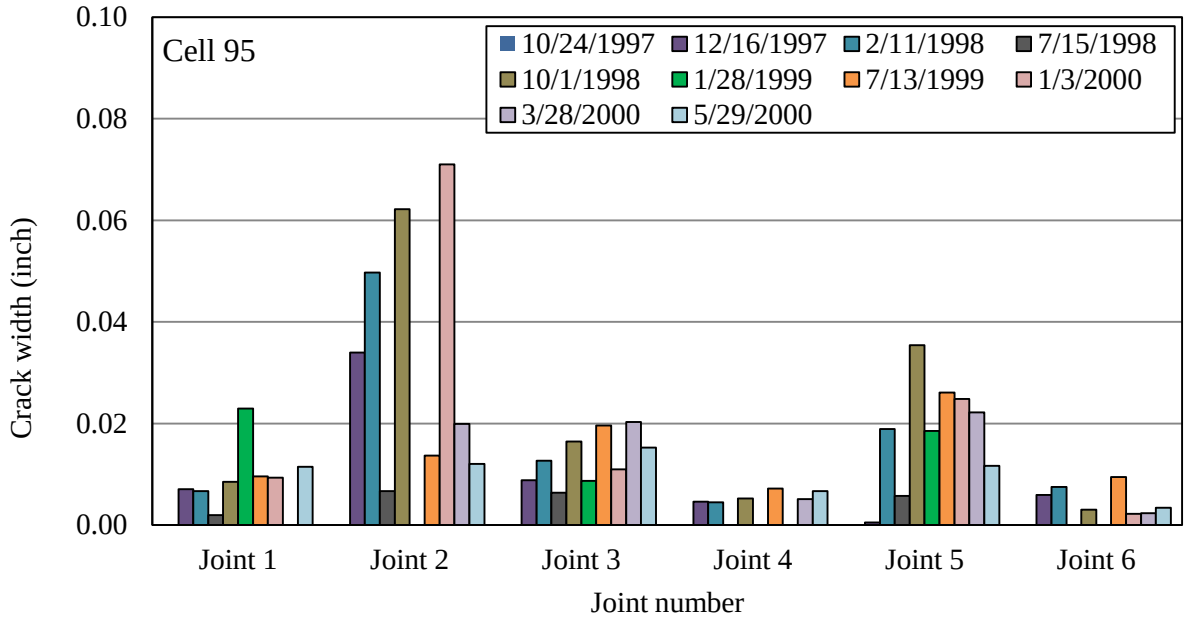

Figure 2-12: Crack width at different joints in MnROAD Cell 95.

2.7 Influence of Joint Performance

The joint performance influences the integrity of the entire overlay system and contributes to the initiation of distresses. Poor joint performance mainly influences (i) debonding of the HMA layer from the UTW and (ii) the load related stress under the loaded slab. The following subsections describe the influence of joint performance with regards to both of the issues.

2.7.1 Debonding of HMA Layer

Differential deflections plays an important role in debonding of the HMA layer from the concrete overlay. Normally, on the loaded side of the joint, the concrete slab and HMA layer are directly deflected under the compression exerted by the wheel load. The deflections exhibited by both the layers are same as a result. The stress at the interface (in the vertical direction) is compressive in nature. At the unloaded side, the nature and magnitude of the stress at the interface depend on the magnitude of differential deflection. In general, this stress would be tensile in nature in this case. The tensile stress is referred as the 'debonding stress.' Figure 2-13 shows the probable scenarios when the joint performance is high and low. At a high joint performance (Figure 2-13 a), the overlay and the HMA layer at the unloaded side exhibit a

similar deflection that the loaded side layer exhibits. The debonding stress at the interface is lower in this case. At a low joint performance (Figure 2-13 b), the deflection on the unloaded slab side is lower than the deflection on loaded slab side. Since, the HMA layer is a continuous layer, the wheel load generated tensile stress tends to debond the HMA layer from the overlay, on the unloaded side. The magnitude of the minimum tensile stress that can contribute to debonding will be referred to as 'peeling stress'. The magnitude of the peeling stress is also a function of the existing interface bonding condition. When both the existing interface bonding condition and joint performance are good then a relatively higher debonding stress is required to peel off or debond the HMA layer from the overlay.

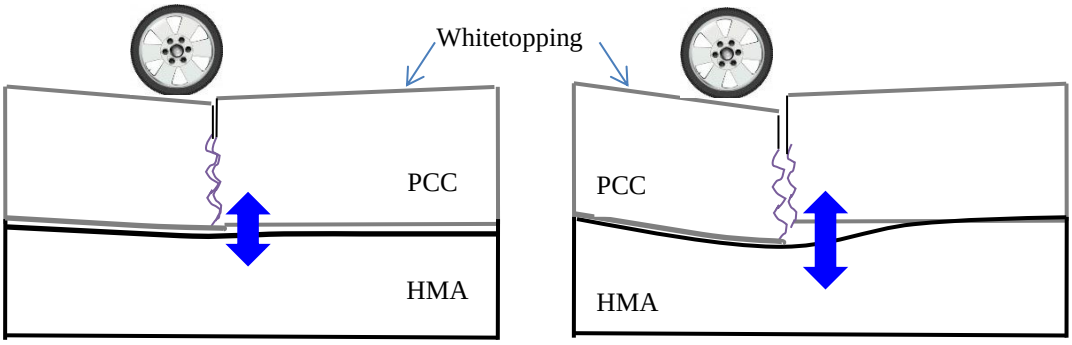

Figure 2-13: Schematic of debonding stress at the interface (a) Higher joint performance, (b) Lower joint performance.

2.7.2 Stress in the loaded slab

At a better joint performance, when the joint shear stiffness is higher, larger percentage of the wheel load is transferred to the adjacent slab, or it can be said that the wheel load is distributed over a larger area. This reduces the stress on the loaded slab, which is responsible for the initiation of distress. Figure 2-13 schematically shows the higher and lower load related stress at the bottom of overlay at low and high joint performance conditions, respectively. It may also be added that at a good joint performance when the layers are properly bonded, the neutral axis of bending shifts downward resulting in a lower tensile stress at the bottom of whitetopping.

2.8 Joint Performance Evaluation Procedures in Literatures

The joint performance for an in-service pavement is typically evaluated by non-destructive methods. Usually falling weight deflectometer (FWD) testing is utilized to measure the deflections on both sides of the joint under a dynamic load. These deflections are used to calculate the LTE. Such evaluations are very helpful in determining the structural condition of the joints for in-service pavements. However, this information does not become available during the design process. It would be a great opportunity if the joint performance behavior of the concrete to be used is known during the design process. The joint performance in regards to different variables, such as aggregate and concrete properties, crack width and crack face texture, will be great information to put into the design procedure. Different researchers thereby proposed different laboratory procedures to characterize the joint performance of concrete. This section describes a few laboratory joint performance test setups developed by different researchers.

Colley & Humphrey, 1967, and Nowlen, 1968 developed a laboratory joint performance test setup, as shown in Figure 2-14. This setup was utilized to establish the effect of crack width on the joint performance through the aggregate interlock mechanism. Two types of subbase (i) 6-in thick sand gravel and (ii) 6-in thick cement treated gravel were considered. The schematic of the instrumentations on the test slabs is shown in Figure 2-15. Loading was applied through two actuators providing 9-kip loads, at a designed phase difference. The time difference between the two peak loads was 0.02 seconds, simulating a 30 mph vehicle speed. The applied load profiles and the resulting deflection profiles on the approach and leave slabs are shown in Figure 2-16.

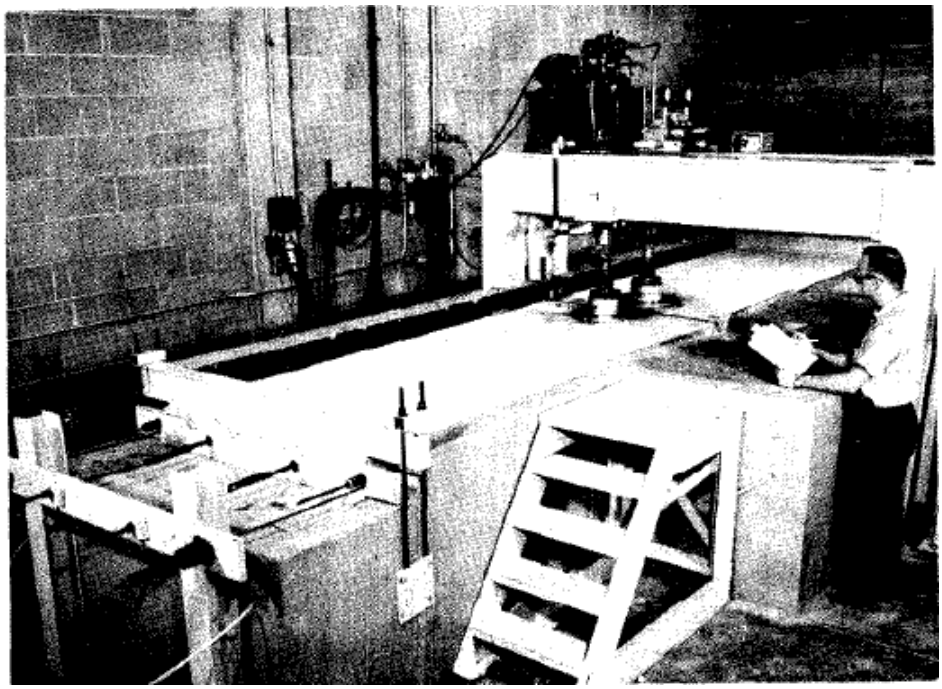

Figure 2-14: Joint performance evaluation setup (Colley & Humphrey, 1967 and Nowlen, 1968).

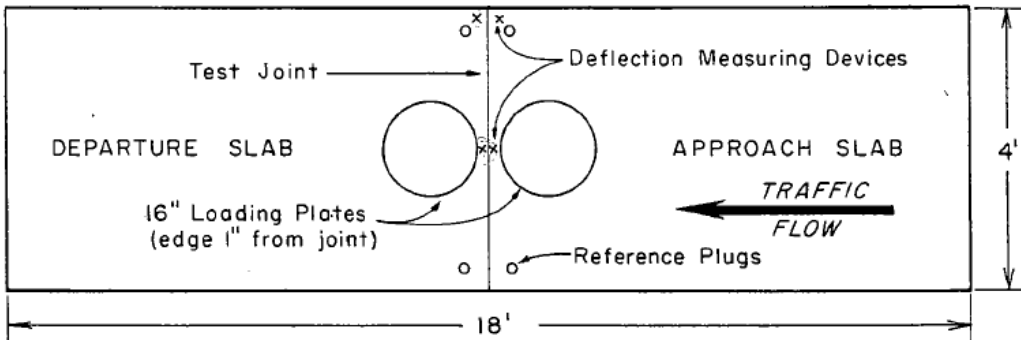

Figure 2-15: Schematic of the instrumentations on the test slabs (Colley & Humphrey, 1967 and Nowlen, 1968).

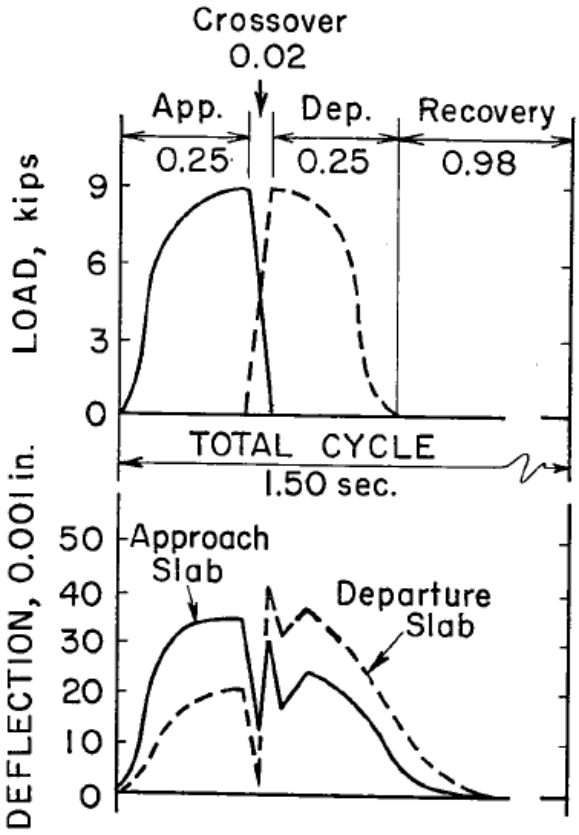

Figure 2-16: Load and deflection profiles (Colley & Humphrey, 1967 and Nowlen, 1968).

Raja & Snyder, 1995 studied the joint performance behavior of jointed reinforced concrete pavement (JRCP) slabs. In that study, joint performance of the slabs cast with different types of aggregates were investigated. Figure 2-17 is a schematic of the test stand used in their study. The foundation support under the test slab was provided by layers of elastomeric neoprene pads. The stiffness of the neoprene pad was equivalent to the composite stiffness of the granular layers beneath the slab. Two different stiffnesses equivalent to 100- and 250-psi/in moduli of subgrade reaction (k) were considered. The slabs were tested with a sinusoidal loading profile as shown in Figure 2-18. The deflections of the loaded and unloaded slabs were measured to estimate the LTE at different crack widths and load repetitions.

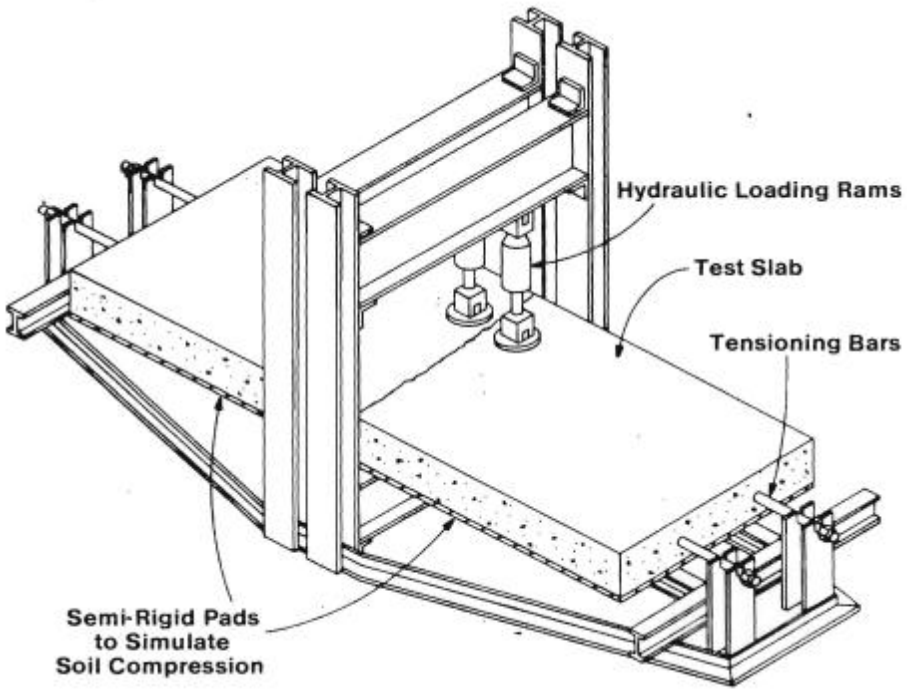

Figure 2-17: Schematic of the joint performance test frame in Raja & Snyder, 1995 study.

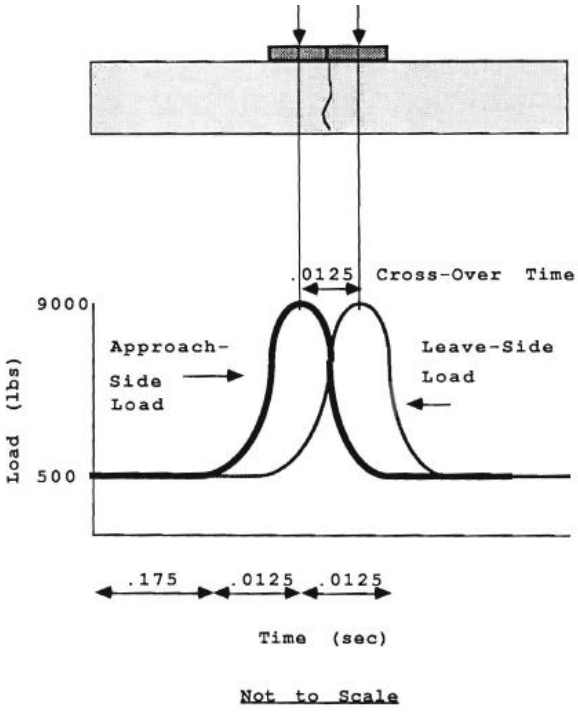

Figure 2-18: Load profile in Raja & Snyder, 1995 study.

A large-scale laboratory slab testing system was developed by Jensen & Hansen, 2001 as shown in Figure 2-19. The instrumentation on the test slabs is shown in Figure 2-20. In this study, the

instrumented slab was placed on a 4-in open graded drainage course on a 16-in thick subbase. The vehicle wheel load was simulated by a single actuator. The magnitude and frequency of the applied load were 9-kip and 3 Hz, respectively. LTE was measured at different crack widths.

Figure 2-19: LTE test frame in Jensen & Hansen, 2001 study.

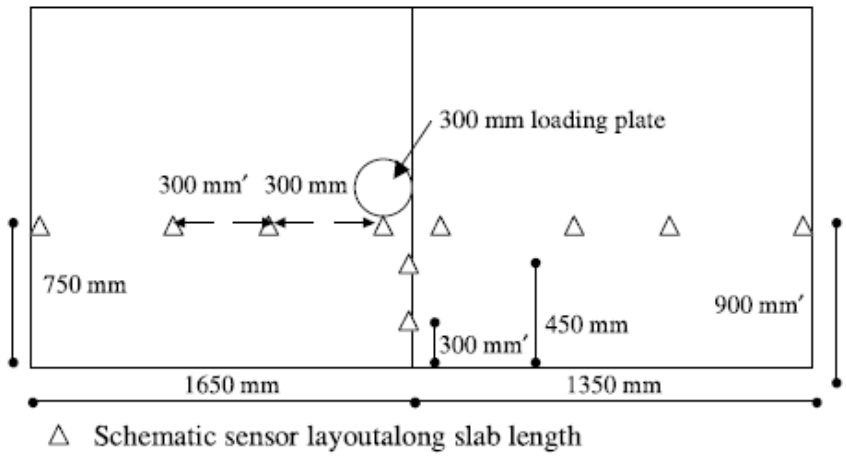

Figure 2-20: Slab instrumentation of joint performance test at Jensen & Hansen, 2001 study.

Brink, et al., 2004 conducted a joint performance study on 9-in thick slabs placed on an artificial foundation. The artificial foundation simulating the subbase support was prepared by using a 2-in thick re-usable rubber layer. The rubber layer provided a composite modulus of subgrade reaction equal to 300 psi/in. A schematic layout of the test setup can be seen in Figure 2-21.

Similar to the Colley & Humphrey, 1967 and Raja & Snyder, 1995 joint performance studies, the vehicle load was simulated using two actuators, with a 9-kip peak load on each actuator. The peak loads on the actuators were applied in the form of a sinusoidal loading, with a phase difference, so that a 50 mph vehicle speed is simulated. The dynamic load frequency was 3 Hz. Static and dynamic load transfers and the relative movement of the slabs were measured at different crack widths.

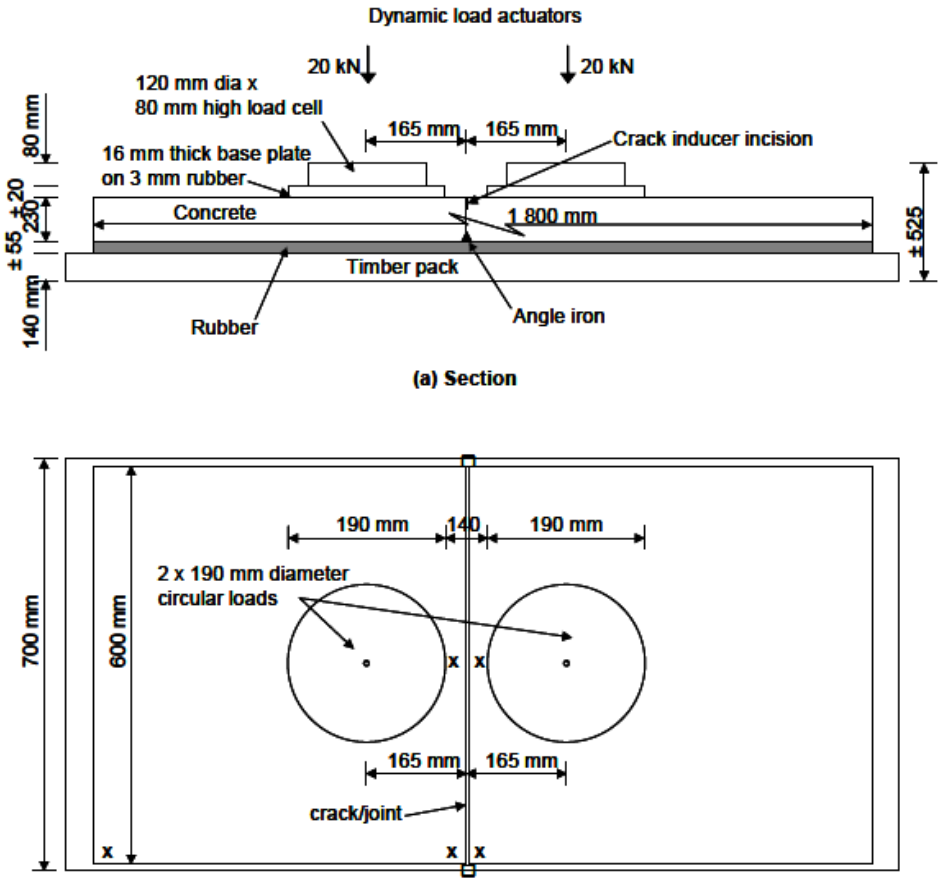

Figure 2-21: Schematic lay out of Brink, et al., 2004 study.

Arnold, et al., 2005 developed a small-scale laboratory joint performance test setup. Using this setup, a half-scale prism specimen was used for evaluating joint performance. In this procedure, 16- x 4- x 4-inch beams were cracked at two locations, as shown in Figure 2-22. Upward and downward load cycles were applied at the center piece of the beam to create a mechanical action that simulates a vehicle passing the approach and leave slabs. The main disadvantage of this test setup is the avoidance of a foundation layer. The load magnitude was determined by simulating the equivalent mechanical action of an in-service condition. Three different load magnitudes were considered, which includes ± 0.45 kip, ± 0.90 kip and ±1.35 kip. This was to simulate ± 5.6 kip, ± 11.2 kip and 16.8 kip loads. The sinusoidal load profile that was used in the study can be seen in the Figure 2-23.

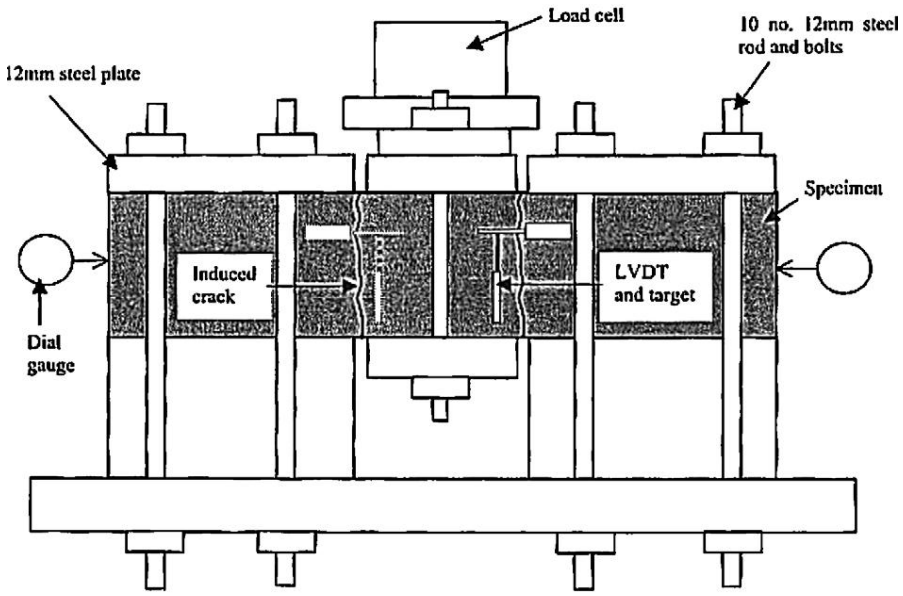

Figure 2-22: Joint performance test setup (Arnold, et al., 2005).

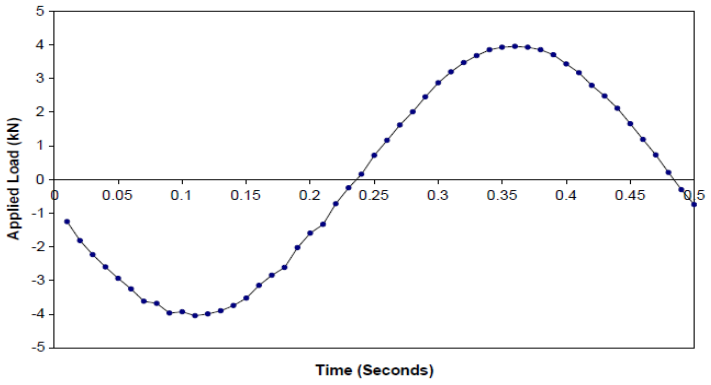

Figure 2-23: Load profile in Arnold, et al., 2005 study.

2.9 Factors Influencing Joint Performance

The factors influencing the joint performance are discussed in this section. The main factor contributing to joint performance is the aggregate interlock, apart from the dowel action provided by the dowel bars or fibers, if any. The joint performance by aggregate interlock is a function of crack width and surface texture of the cracked face. The following subsection introduces the different factors that influence the aggregate interlock.

2.9.1 Volumetric surface texture

A larger amount of texture on the surface of the crack face of the slab results in a higher joint performance by engaging more aggregate particles in transferring the load. Vandenbossche, 1999 proposed a relationship to establish the joint performance based on surface texture and crack width (cw). Surface texture is quantified using the volumetric surface texture ratio (VSTR). It is the volume of texture per unit surface area of the crack face. In volumetric surface texture (VST) test, the distance (d_i) of the crack surface from an arbitrarily selected datum is measured by using a probe or a laser profiler. Figure 2-24 shows a VST test setup used in the Vandenbossche, 1999 study. Generally, the crack face is divided into equal grids. Distance is measured at the center of each grid. A graphical representation of the VSTR measurements and calculations can be seen in Figure 2-25. The average distance (d_{avg}) of the individual distances (d_i) is calculated as follows:

$$d_{avg} = \frac{\sum_{1}^{n} d_i}{n} \tag{2-6}$$

where n is the number of the grids on the crack surface. The residual (r_i), which is the difference between the average distance and distance of individual grids (d_i), is calculated by the following Equation.

$$r_i = d_i - d_{avg} \tag{2-7}$$

Then, the volume of each individual grid is calculated by using Equation (2-8).

$$V_i = r_i * A_i \tag{2-8}$$

where is V_i is the volume and A_i is the area of each grid on the crack surface. A positive value of V_i represents the volume of texture above the plane determined by $d_{avg.}$ A negative value of V_i represents the volume of the texture below the plane. The algebraic sum of V_i obtained for each grid provides the volume of surface texture (*VST*) as given by the following Equation.

$$VST = \sum_{1}^{n} abs(r_i * A_i) \tag{2-9}$$

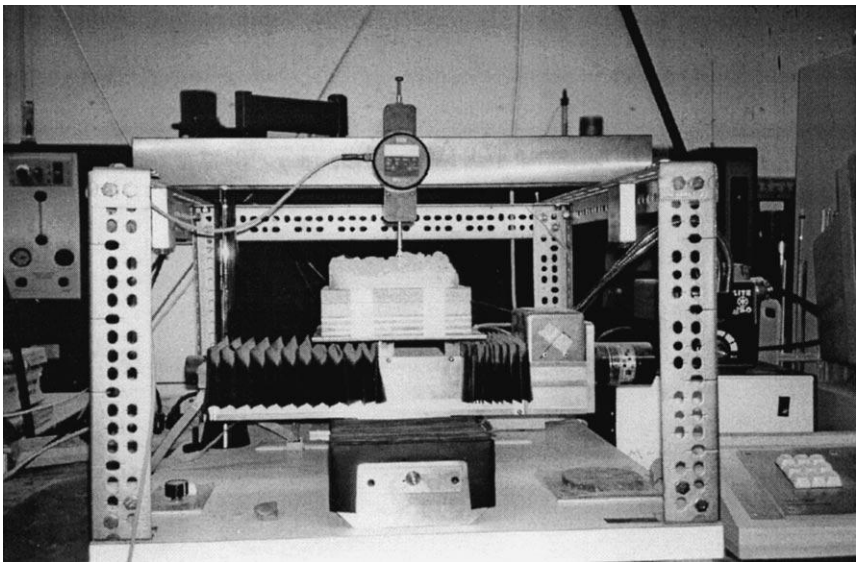

Figure 2-24: VST test setup in the Vandenbossche, 1999 study.

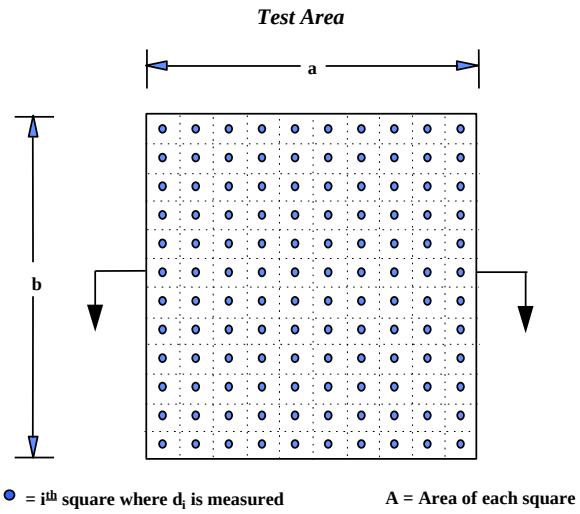

Figure 2-25: Graphical representation of VSTR measurements in Vandenbossche, 1999 study.

Vandenbossche, 1999 developed a relationship for the LTE as a function VST normalized by cw. Figure 2-26 presents the relationship that was developed with the laboratory test results. The proposed model is given by the Equation (2-10).

$$LTE = 39.7 \cdot \log\left(\frac{VSTR}{cw}\right) + 5.6 \qquad (2\text{-}10)$$

where *LTE* is the deflection load transfer efficiency in percentage, VST is the volumetric surface texture in cm^3/cm^2 and *cw* is the crack width in cm.

Figure 2-27 presents the relationship between the *VST* and *AGG*. Laboratory test results were used to develop this model. The regression model is given in Equation (2-11).

$$AGG = 105.72e^{2.367\log(VST/cw)} \quad (2\text{-}11)$$

where *AGG* is the joint spring stiffness expressed in kPa/mm, the VST is the volumetric surface texture in cm^3/cm^2.

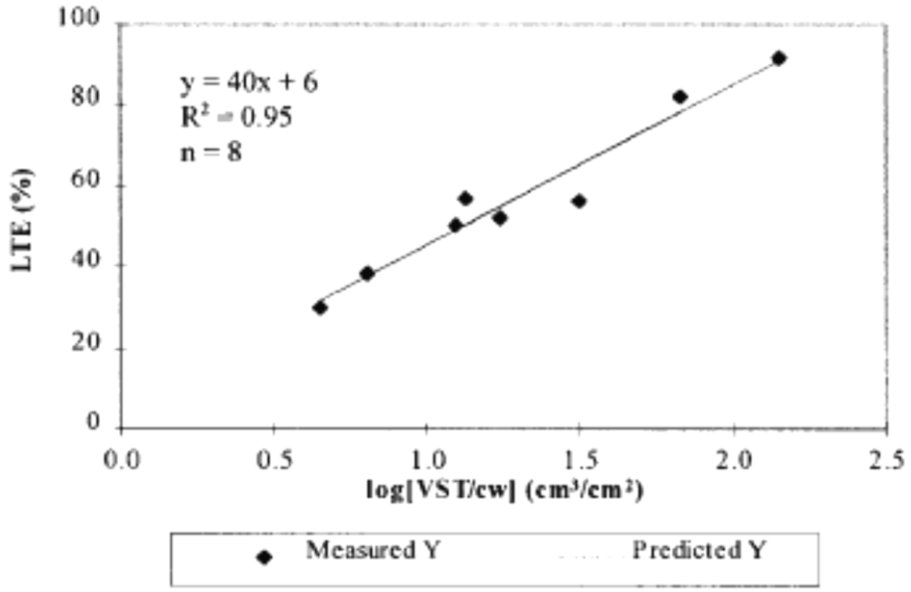

Figure 2-26: Regression model for LTE as a function of VST and cw (Vandenbossche, 1999).

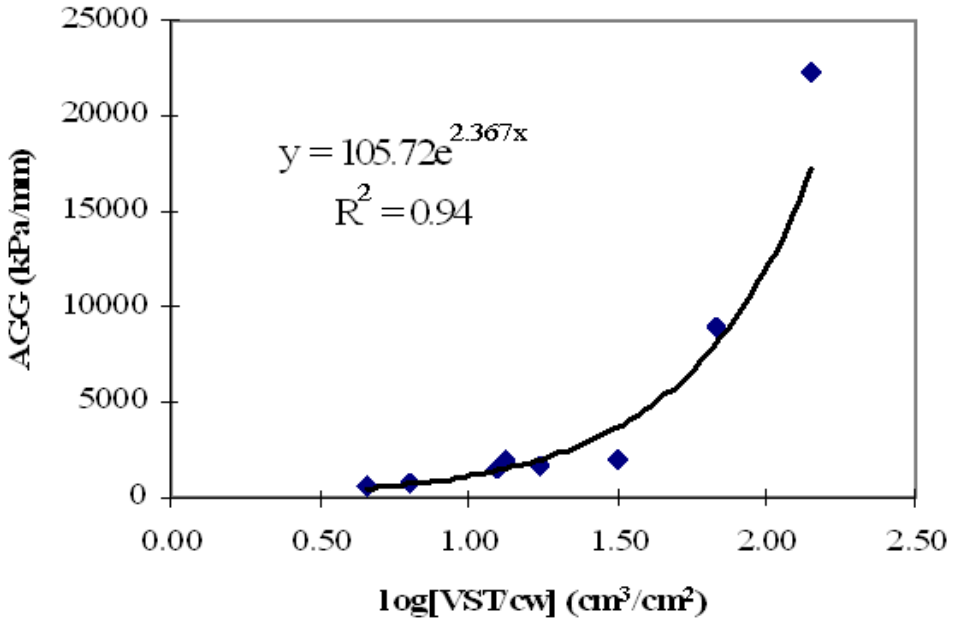

Figure 2-27: Regression model of AGG as a function of VST and cw (Vandenbossche, 1999).

Ramirez, 2010 modified the above model so that *AGG* could be estimated as a function of the depth of texture available at the slab face, ST, in addition to *VST* and *cw*. The modified model is given below.

$$AGG = \left[105.72 * e^{2.367 * \log\left(\frac{VSTR * a * ST}{cw}\right)} \right] * b \qquad (2\text{-}12)$$

where *a* and *b* are constants equal to 2.54 and 3.6838, respectively, for unit conversion(from US customary unit to SI unit), *ST* is the slab thickness in cm and *cw* is the crack width in cm.

The volumetric surface texture is a function of the type, shape, top size, and gradation of the coarse aggregate and the water cement ratio. Since the *VST* influences the joint performance, a discussion on the factors that affects the VST are also included.

Aggregate type

The hardness of the aggregate, which is related to the abrasion resistance capability and toughness, influences the volumetric surface texture. With the presence of harder aggregates in the concrete, the crack meanders around the aggregates and produce a rougher fracture face (Vandenbossche, 1999; Chupanit & Roesler, 2008 and Ramirez, 2010). Figure 2-28 shows examples of fracture faces of concrete with a harder type aggregate, such as limestone, and a softer aggregate, such as slag. The study conducted by Vandenbossche, 1999 indicates that the concrete with the stronger aggregates (limestone in this case) possesses a higher VSTR than that of softer aggregates (gravel or slag in this case). See Figure 2-29. This graph shows the average VSTRs for eight specimens, for a coarse aggregate top size of 1.5 inch. Since, the concrete prepared with harder aggregates as compared to softer aggregates exhibits a higher VSTR, the joint performance is also likely to be improved.

Figure 2-28: Example of fracture surface for two types of aggregates, (after Ramirez, 2010).

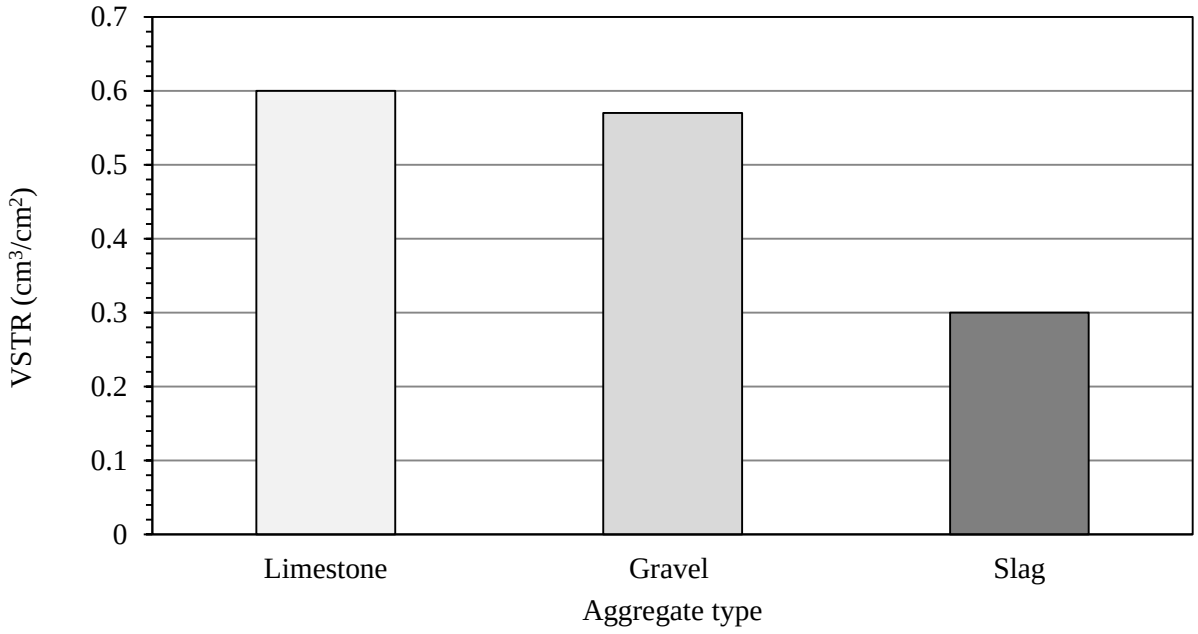

Figure 2-29: Effect of coarse aggregate type on VSTR (after Vandenbossche, 1999).

The study conducted by Raja & Snyder, 1995 also shows that harder aggregates exhibit lower abrasion under load cycles. Figure 2-30 is a comparison of the LTE obtained for virgin gravel, limestone and slag aggregates (Raja & Snyder, 1995). It can be seen that limestone aggregates not only exhibits higher LTE but maintain a higher LTE for a larger number of load cycles. Similar findings were published by Colley & Humphrey, 1967. In Figure 2-31, it can be seen that aggregates with a lower Los Angeles Abrasion value result in a higher joint effectiveness. The joint effectiveness is given by the following equation.

$$E_j = \frac{2d'_u}{d'_u + d'_l} \tag{2-13}$$

where E_j is the joint effectiveness, d'_l and d'_u are the deflections of the loaded and unloaded slab, respectively.

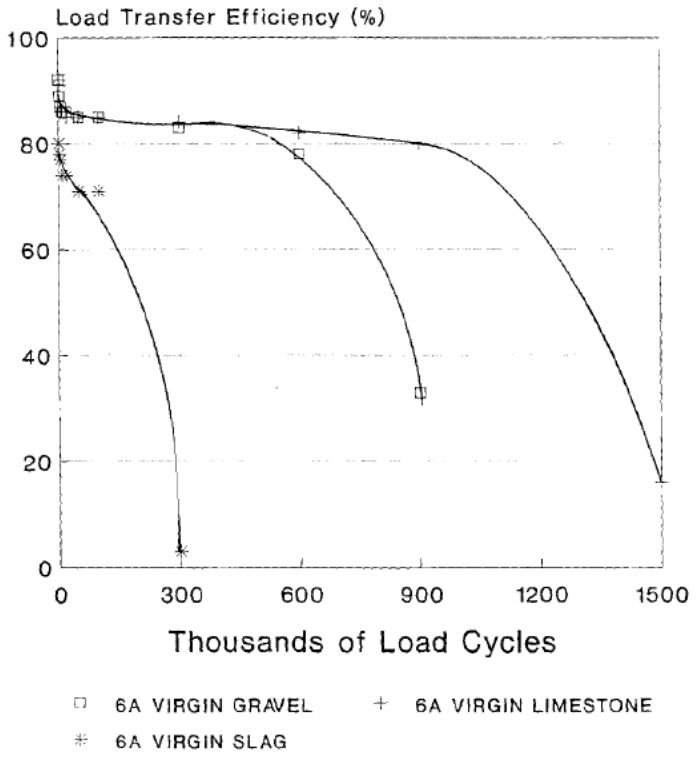

Figure 2-30: Effect of coarse aggregate type on LTE (Raja & Snyder, 1995).

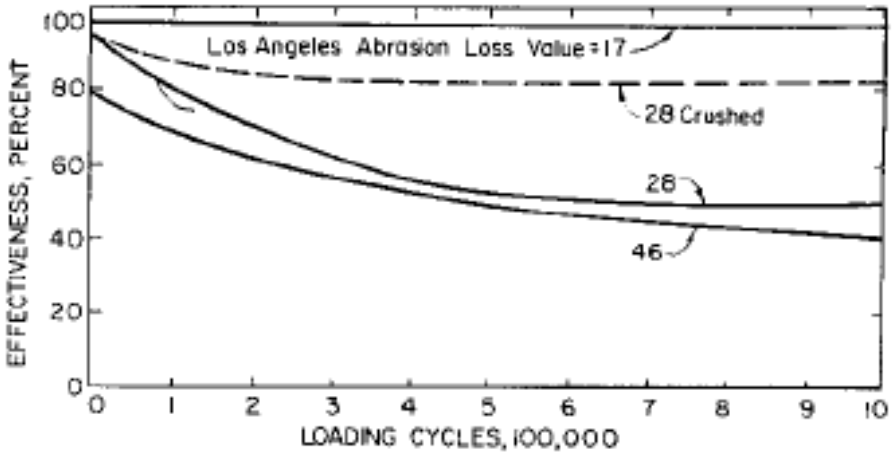

Figure 2-31: Effect of Los Angeles Abrasion value on LTE (Colley & Humphrey, 1967).

Coarse aggregate angularity

Several research studies have shown that the angularity of the aggregates also influences joint performance. Colley & Humphrey, 1967 compared the joint effectiveness of crushed gravel and natural gravel. Figure 2-32 shows that the angular crushed gravel mantians a higher joint effectiveness for a larger number of load cycles than that of the smoother natural gravel.

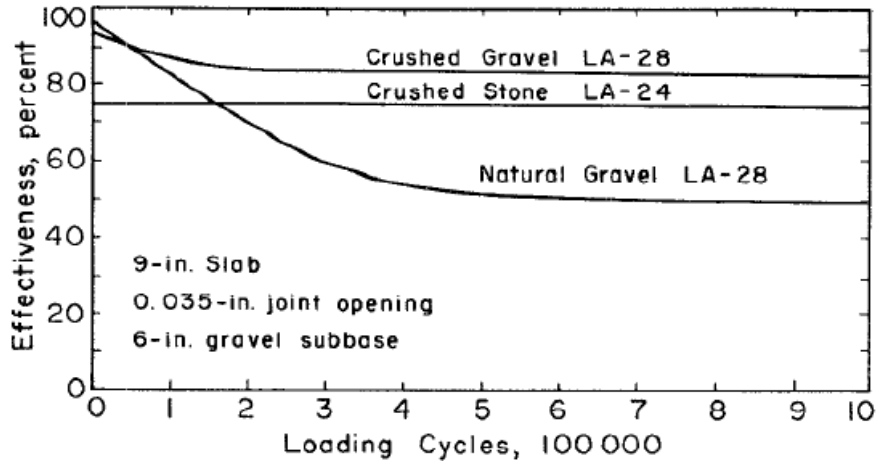

Figure 2-32: Influence of aggregate shape (angularity) on joint effectiveness (Colley & Humphrey, 1967).

Coarse aggregate top size

It is natural that when larger aggregates are used in the mix, the crack becomes more tortuous and results in a higher VSTR when compared to smaller size aggregates (Vandenbossche, 1999; Chupanit & Roesler, 2008; 2005 and Ramirez, 2010). Figure 2-33 shows concrete composed of 2.5-inch top size aggregates results in a higher VSTR than the concrete with 1.5-inch top size aggregate (Vandenbossche, 1999). Since, the VSTR of the concrete with coarser aggregates is higher, it is natural that joint performance will also be higher (Nowlen, 1968, Raja & Snyder, 1995, Jensen & Hansen, 2001).

Figure 2-34 shows that 1-in gravel results in a higher LTE than a 0.75-in gravel aggregates (Raja & Snyder, 1995). The findings published by Colley & Humphrey, 1967 also support this fact. In Figure 2-35, it can be seen that the concrete composed of 2.5 in top size aggregates, as compared to 1.5 and 0.75 in top size aggregates, resulted in a higher joint effectiveness.

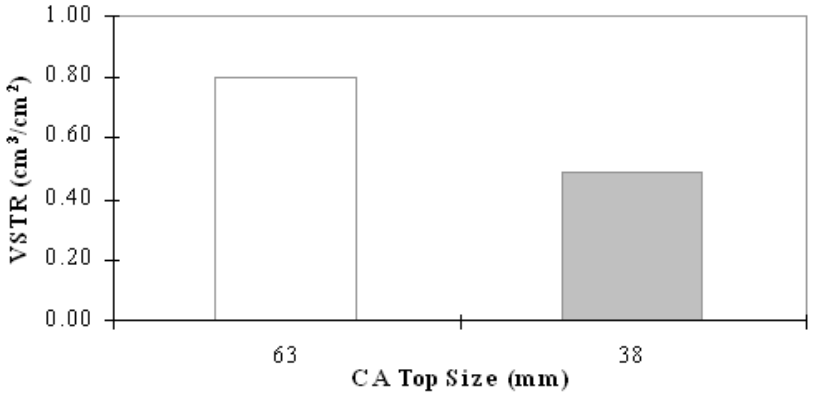

Figure 2-33: Effect of coarse aggregate top size on VSTR (Vandenbossche, 1999).

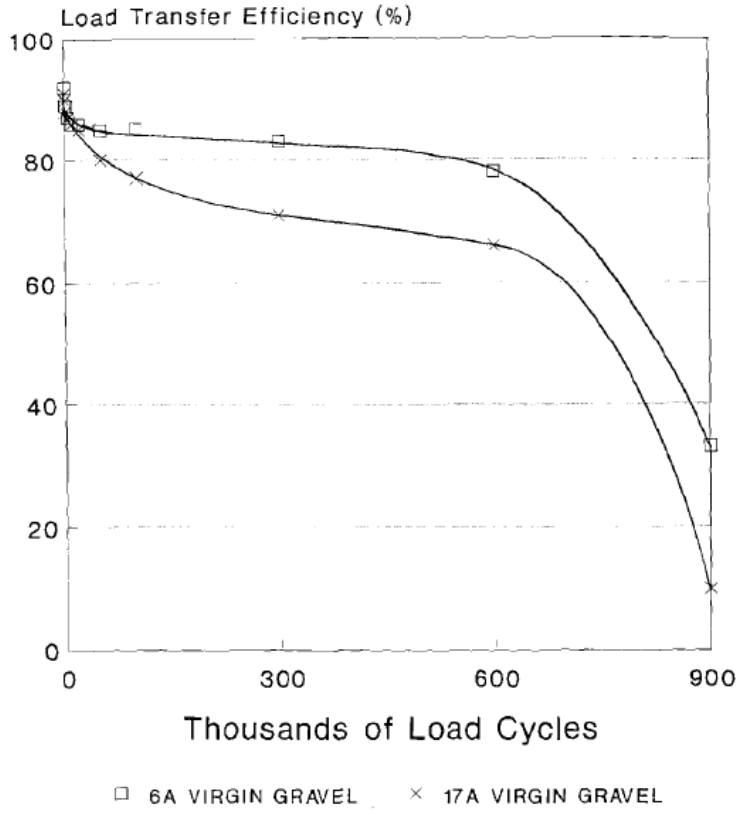

Figure 2-34: Influence of aggregate top size on LTE (Raja & Snyder, 1995).

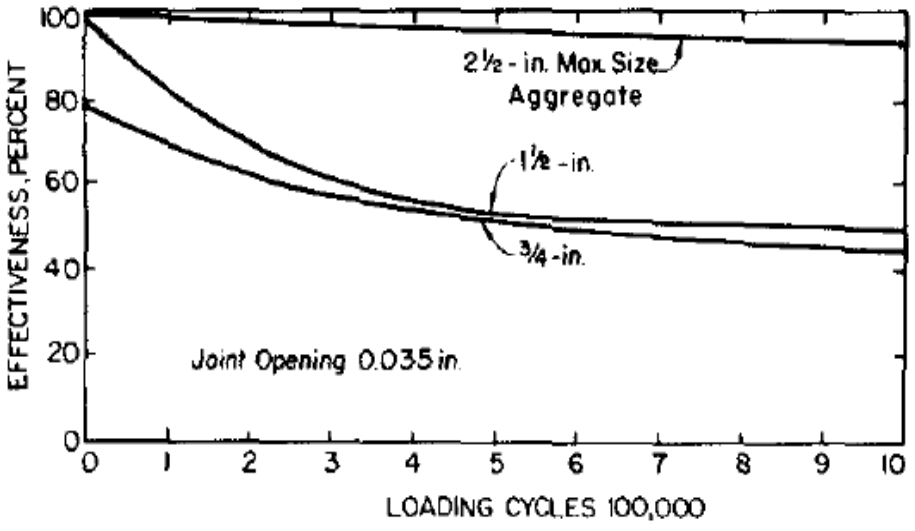

Figure 2-35: Influence of aggregate top size on joint effectiveness (Colley & Humphrey, 1967).

Coarse aggregate gradation

Aggregate gradation may also influence the surface texture of the fractured face. Unfortunately, only a very limited study is available to draw a sound conclusion about the sensitivity of the aggregate gradation. Chupanit & Roesler, 2008 conducted a study with a gap and dense graded aggregate. They concluded that the matrix with a gap gradation when compared to a dense gradation, exhibits slightly higher VSTR.

Age at crack initiation

The time of cracking of the specimen is an important factor that influences the meandering of the crack. Nowlen, 1968 found that inducing cracks in the specimen at an early age results in a higher joint performance than when the specimen is cracked at a later age. At an early age, the strength of the matrix remains lower than that of the strength of the aggregates. That is why when the concrete is cracked at an early age, cracks form around the aggregates and not through the aggregates. Figure 2-36 shows the joint effectiveness vs load cycle relationship for the concrete (with similar mix proportion) cracked at three different ages. This study was conducted on a 9-in concrete slab on top of a 6-in gravel subbase. The crack width was 0.035 in. It can be seen that the slab cracked after 7 days resulted in a lower load transfer when compared to the slabs cracked after 1- and 3-days.

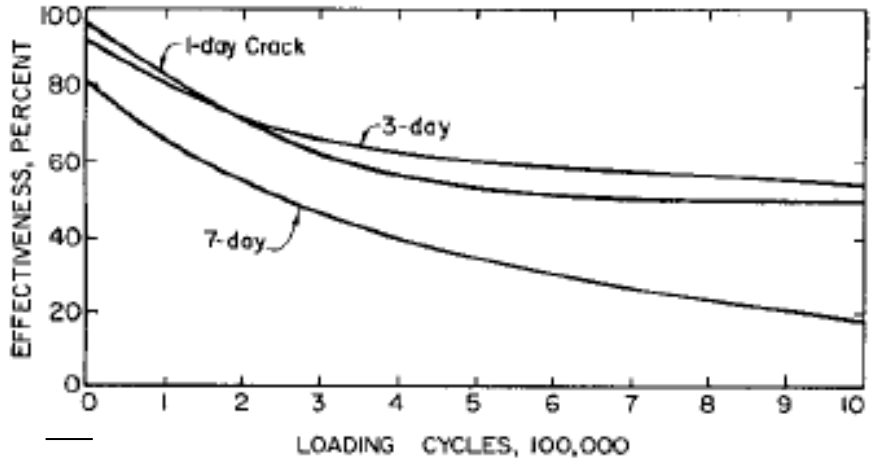

Figure 2-36: Influence of time of cracking on joint effectiveness (Nowlen, 1968).

2.9.2 Crack width

Perhaps the most important variable that influences the joint performance is the crack width. Several studies have been conducted to establish the joint performance vs crack width relationship considering different pavement conditions, such as different support conditions, aggregate types and load cycle numbers (Benkelman, 1933, Colley & Humphrey, 1967; Hansen, et al., 1998 and Jensen & Hansen, 2001).

In a study conducted by Hansen, et al., 1998, it was found that the joint performance starts decreasing at a crack width greater than 0.025 in. See in Figure 2-37. In the Jensen & Hansen, 2001 joint performance study (setup was discussed in Section 2.8), three significant stages of load transfer were identified, as shown in Figure 2-38. At stage I when the crack width remains lower than 0.02 in, the LTE is almost 100%. The load transfer at a crack width between 0.025 in and 0.10 in is referred as stage II. At this stage, the aggregate interlock is very important. Figure 2-38 and Figure 2-39 show the normalized deflection vs crack width and LTE vs crack width, respectively. The magnitudes of the loaded side deflection and the differential deflection increase with increases in crack width. However, the trends are not the same for different aggregates (compare Figure 2-38 a and b) and aggregate top sizes (compare Figure 2-38 b and c). This study also compared the LTE vs cw relationship for two aggregate top sizes. The drop in LTE is lower in the case of 2-in glacial gravels as compared to 1-in glacial gravels. The load transfer at a crack width beyond 0.10 in is referred as stage III. At this stage, aggregate interaction basically diminishes and load is transferred primarily through the foundation.

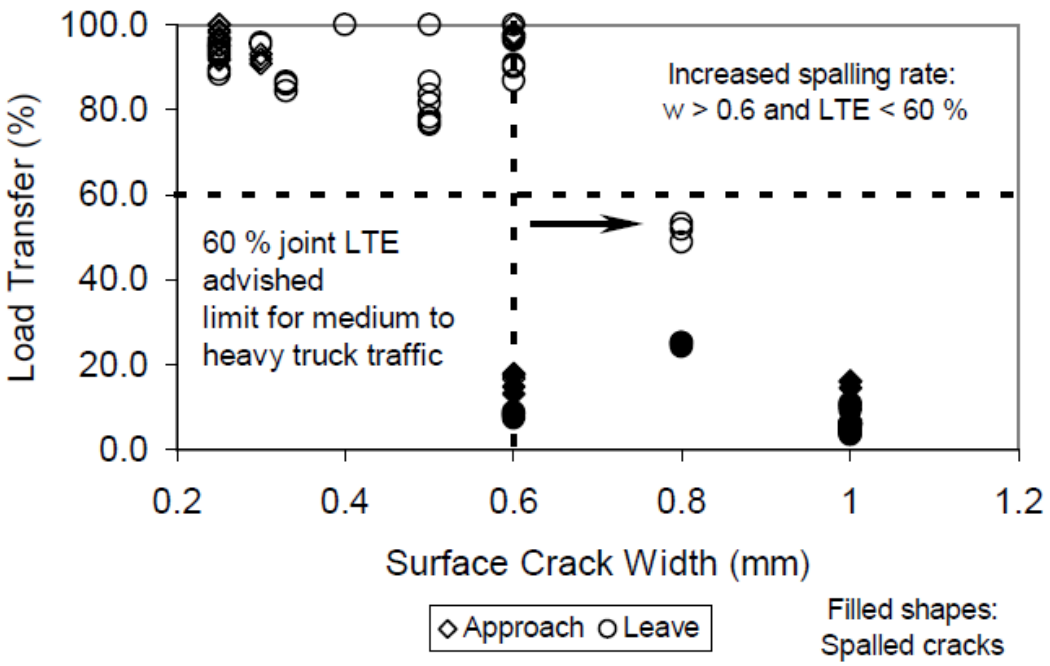

Figure 2-37: Load transfer vs crack width from the field observations from six different JRCPs (Hansen, et al., 1998).

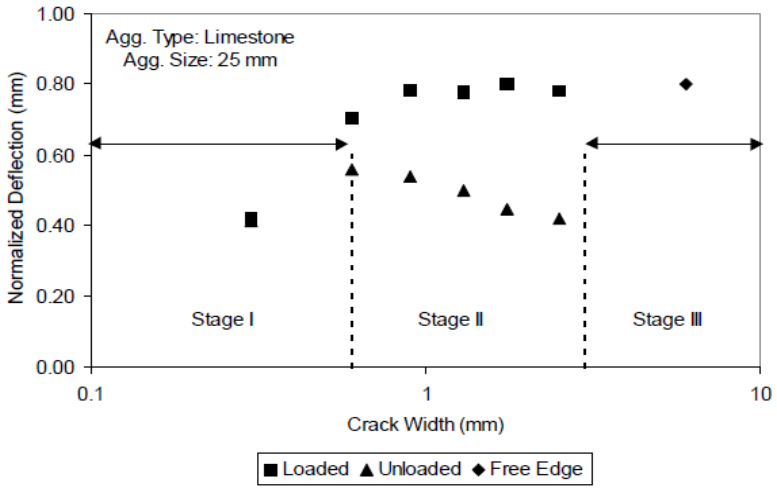

(a)

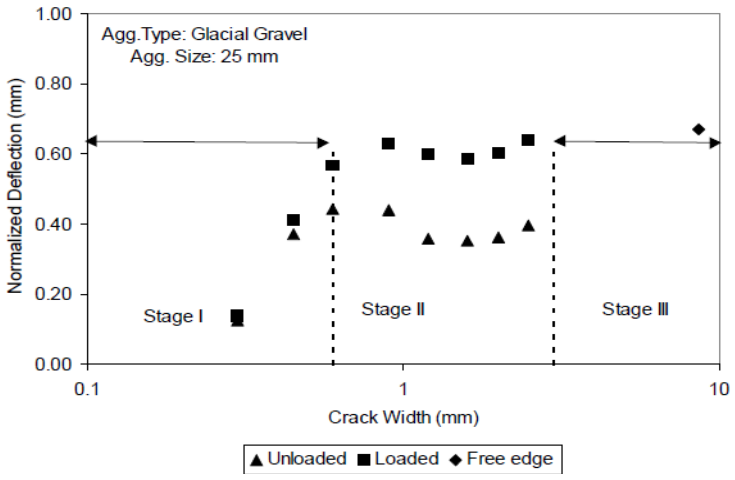

(b)

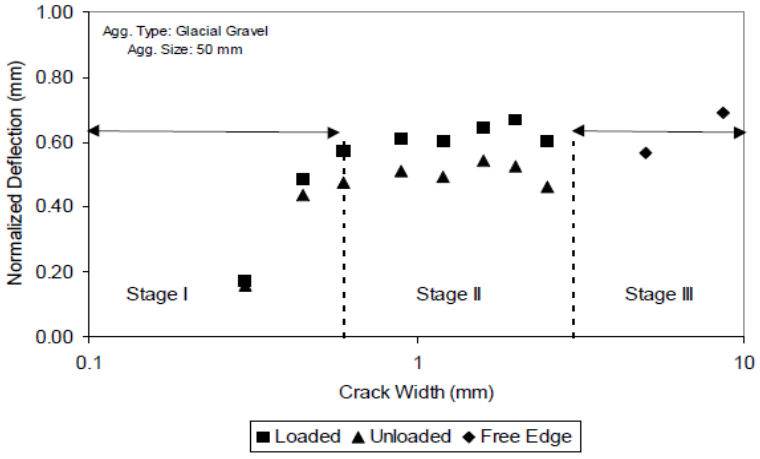

(c)

Figure 2-38: Normalized deflection vs crack width (a) 1- inch limestone, (b) 1- inch glacial gravel and (c) 2-inch glacial gravel (Hansen, et al., 1998).

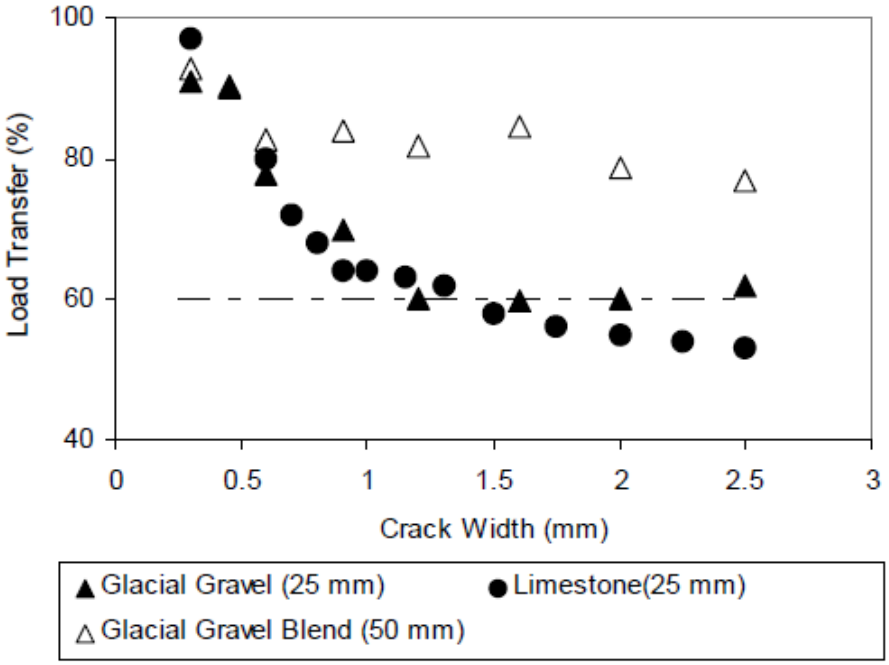

Figure 2-39: Load transfer vs crack width for different aggregate types (Jensen & Hansen, 2001).

The effect of crack width on the joint performance was also characterized by Nowlen, 1968, as shown in Figure 2-40. The laboratory test setup for that study was discussed in Section 2.8. The joint effectiveness was found to be twice as high when the crack width was 0.035 in, as compared to 0.065 in, for a range of aggregate top sizes. Colley & Humphrey, 1967 and Nowlen, 1968 conducted tests on instrumented 7- and 9-in thick slabs. Figure 2-41 presents the relationship between the joint effectiveness, crack width and number of 9-kip load cycles for 7-in thick slabs. It can be seen that for a narrow crack width like, 0.015 in, the joint effectiveness does not drop with the number of load cycles. However, when the crack increases, the joint effectiveness rapidly declines.

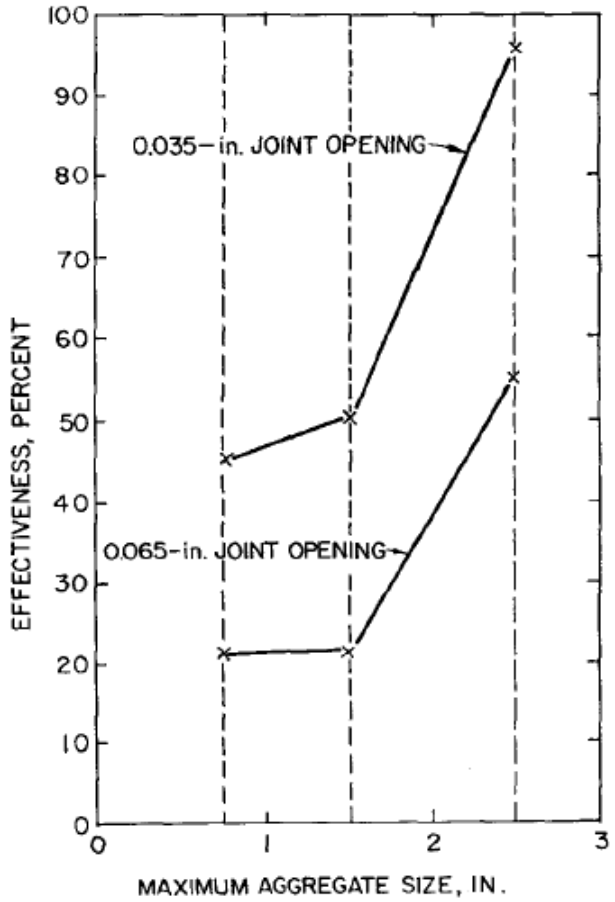

Figure 2-40: Joint effectiveness vs crack width for different aggregate top sizes (Nowlen, 1968).

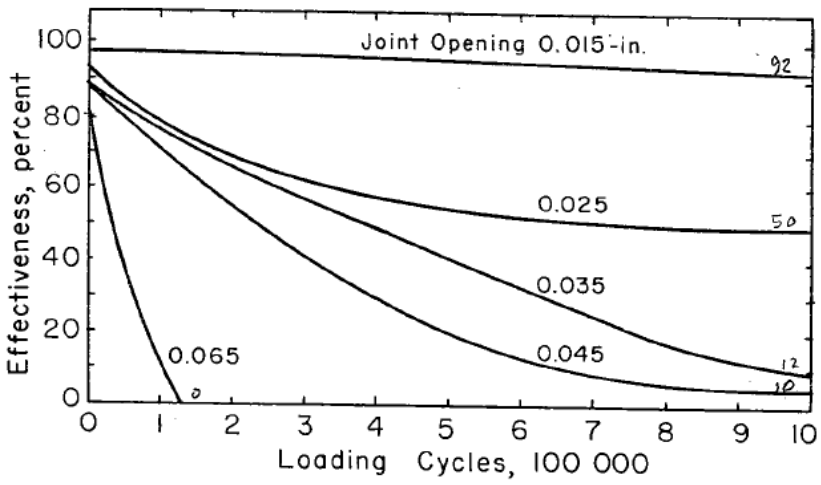

Figure 2-41: Joint effectiveness vs joint opening at different number of load cycles for 7 inch slab (Colley & Humphrey, 1967).

In the Brink, et al., 2004 study, the joint performance vs crack width relationship was investigated for two different aggregate top sizes and two aggregates types. The test setup was discussed in Section 2.6. The LTE vs crack width relationship was relatively different in this study as compared to the previously discussed studies. It can be seen in Figure 2-42 (1.5 in aggregate top size), that the dynamic LTE dropped only by approximately 4 percent when the crack width increased from 0.004 in to 0.100 in. Although the exact reason is not known, the low LTE drop could be due to the use of very small slab sizes (3 ft x 2 ft). See Figure 2-21. The far end unrestrained transverse edges of both the loaded and unloaded slabs most likely lifted up under the dynamic load. In this condition, the differential deflection, which is referred as the relative movement by Brink, et al., 2004 is less dominated by the joint shear stiffness. This probably resulted in a very low variation in the relative movements regardless of the crack widths, as shown in Figure 2-43.

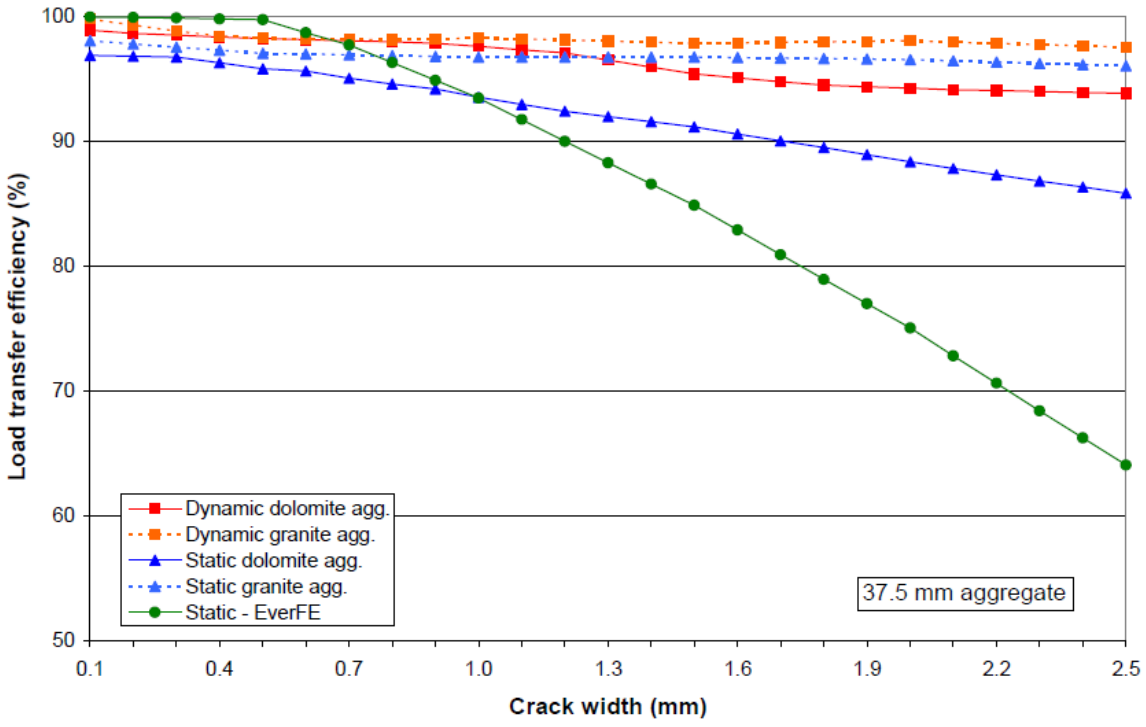

Figure 2-42: Load transfer vs crack width (Brink, et al., 2004).

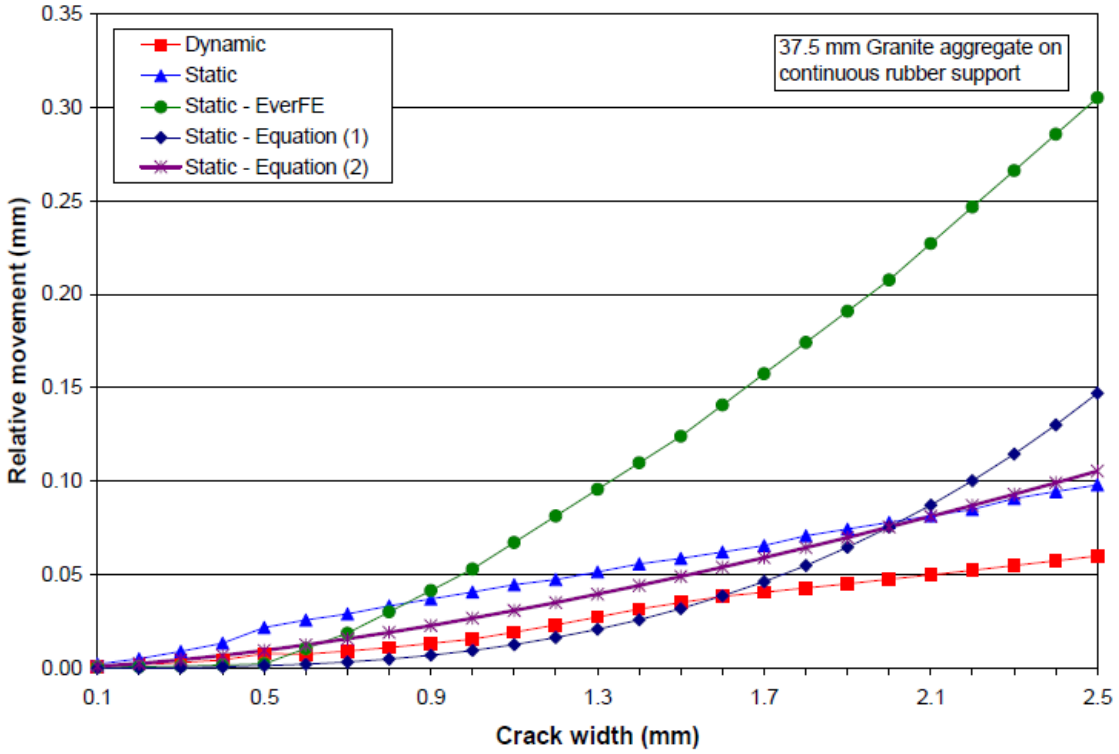

Figure 2-43: Relative movement vs crack width (Brink, et al., 2004).

2.9.3 Number of load applications

The aggregates at the joint abrade with accumulated load cycles (Colley & Humphrey, 1967 and Nowlen, 1968). The magnitude of the abrasion with respect to load cycle depends on the crack width and strength of the aggregates. As was shown in Figure 2-41, the joint effectiveness declination with respect to load cycle was large when the crack width was larger. At a 0.045 in crack width (Figure 2-41), the joint effectiveness dropped by 80 percent as compared to only 6 percent when the crack width was 0.015 in, after 100,000 load cycles. Brink, et al., 2004 reported that at a crack width less than 0.010 in, the load transfer drop was negligible even after 2 million load cycles. At a narrower crack width, the differential deflection remains very low. The mechanical action on the aggregates is also low as a result.

2.9.4 Thickness of the slab

Colley & Humphrey, 1967 and Nowlen, 1968 reported that the joint effectiveness is also a function of the thickness of the slab. Figure 2-41 and Figure 2-44 show that the joint

effectiveness vs. load cycles relationship for 7- and 9-in thick slabs, respectively. For both cases the slab was placed on a 6-in gravel subbase (Colley & Humphrey, 1967). The joint effectiveness was observed to be higher for the thicker slab. A larger crack face area provided by the thicker slab results in a higher joint effectiveness.

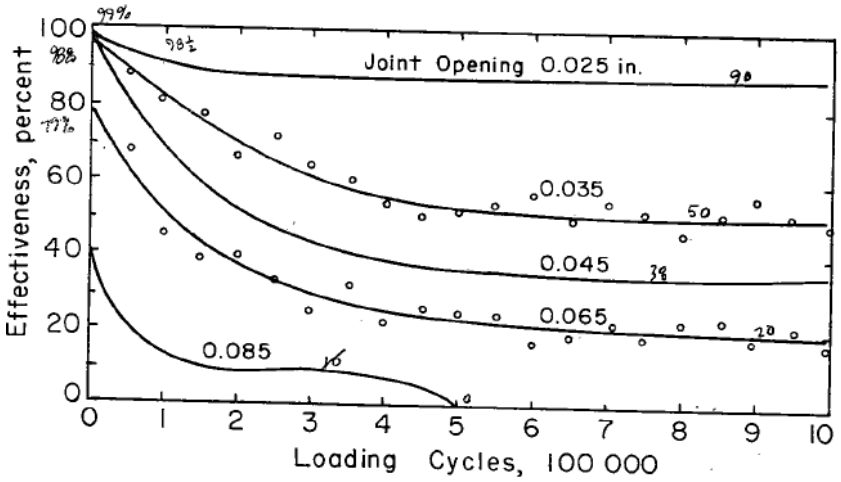

Figure 2-44: Joint effectiveness vs joint opening at different number of load cycles for 9-inch slab (Colley & Humphrey, 1967).

2.10 Fiber Reinforced Concrete in Joint Performance Benefits

The significant role of joint performance in the development of distress in whitetopping is the motivation for investigating feasible ways to increase the joint performance that can be maintained for a longer period of time. Since dowel bars are not used in ultra-thin whitetopping, structural fibers can be a potential alternative. Although many whitetopping projects with FRC have been constructed (Rasmussen, et al., 2002), the benefits of the applications of fibers in increasing the joint performance have actually not been properly investigated. A literature review on the applications of fibers in concrete revealed that both high and low elastic modulus fibers have been used in the construction of UTW. High elastic modulus fibers are generally referred to as structural fibers. These fibers increase the toughness, residual strength, joint stiffness and flexural strength of the concrete (Boredelon, 2005; Rodezno & Kaloush, 2010; Roesler, et al., 2006 and Roesler, et al., 2008). The low elastic modulus fibers, known as non-structural fibers, reduce the plastic shrinkage cracking potential (Naaman, et al., 1984; Zollo & Ilter, 1986; Grzybowski & Shah, 1990; Bentur & Mindness, 1990 and Shah, et al., 1994). The

primarily cracking resistance, impact, wear resistance and ductility of concrete also significantly increase with the addition of fibers (Zhang, et al., 2001). The benefit of the application of fibers in reducing the infiltration or permeability of concrete through the cracks and joints has been reported by many researchers including Aldea, et al., 2000, Rapoport, et al., 2002, Lepech & Li, 2005 and Rajabipour & Akhavan, 2010.

Although both steel and synthetic fibers have been used in the construction of UTW, the use of a synthetic fiber is more common in the United States (Rasmussen & Rozycki, 2004 and Barman, et al., 2010). The difficulties involved in dealing with the heavy weight of the steel fibers during mixing is probably the reason for the less frequent use of steel fibers as opposed to the synthetic fibers. To evaluate the effect of fibers on the joint performance in whitetopping, the performance history of a couple of MnROAD whitetopping sections is reviewed. The performance of two whitetopping sections, one constructed with non-structural polypropylene fibers (Cell 94) and the other constructed with structural polyolefin fibers (Cell 95) are compared. Figure 2-45 shows a picture of the two types of fibers. Joint performance data for these two cells were compared to determine if the slabs in Cell 95 exhibit a higher LTE. It can be seen in Figure 2-46 that the LTEs in Cell 95 were always higher than the LTEs in Cell 94. Another observation is that the contribution of the fibers is more in the winter when the crack width is larger. The slabs with structural fibers had tighter joints than those with the non-structural fibers. The non-structural fibers cannot keep the crack width narrower because of their low stiffness and tensile strength. During the summer time, when thermal expansion forces the joints to be relatively tight, the LTE for the two cells does not differ significantly. Therefore, it can be concluded that structural fibers contribute in increasing LTE.

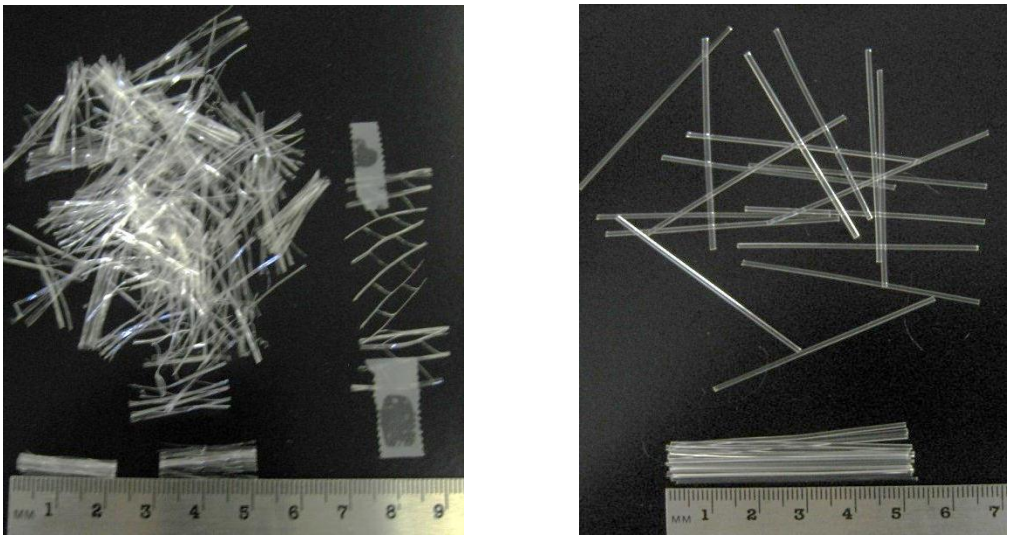

(a) **(b)**

Figure 2-45: Picture of two types of synthetic fibers used in MnROAD Cells 94 and 95: (a) Polypropylene and (b) Polyolefin.

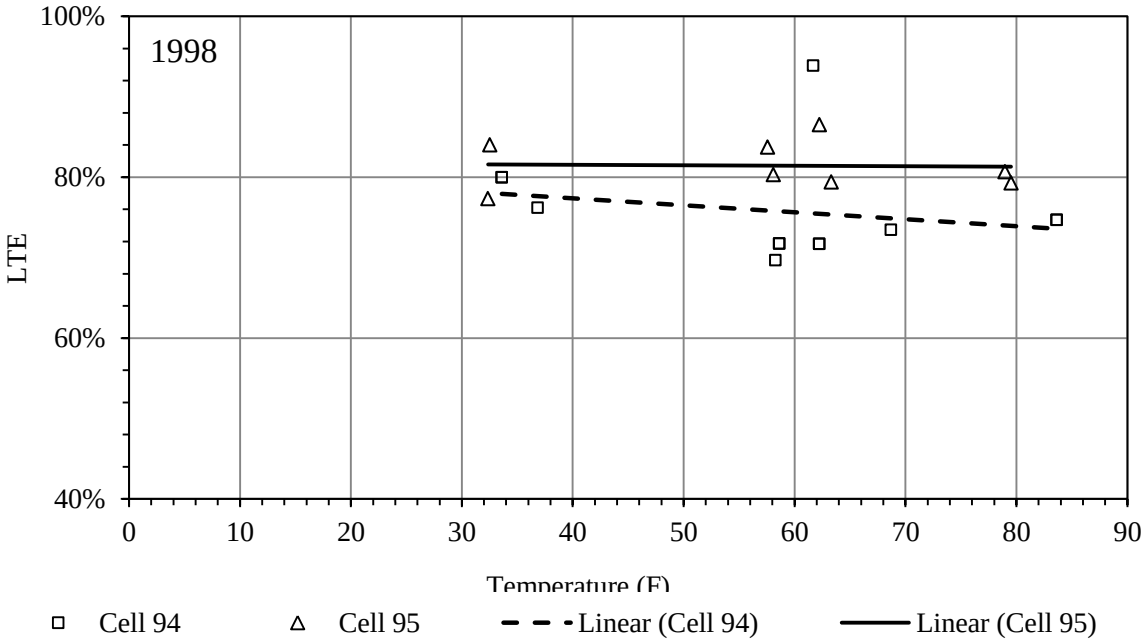

(a)

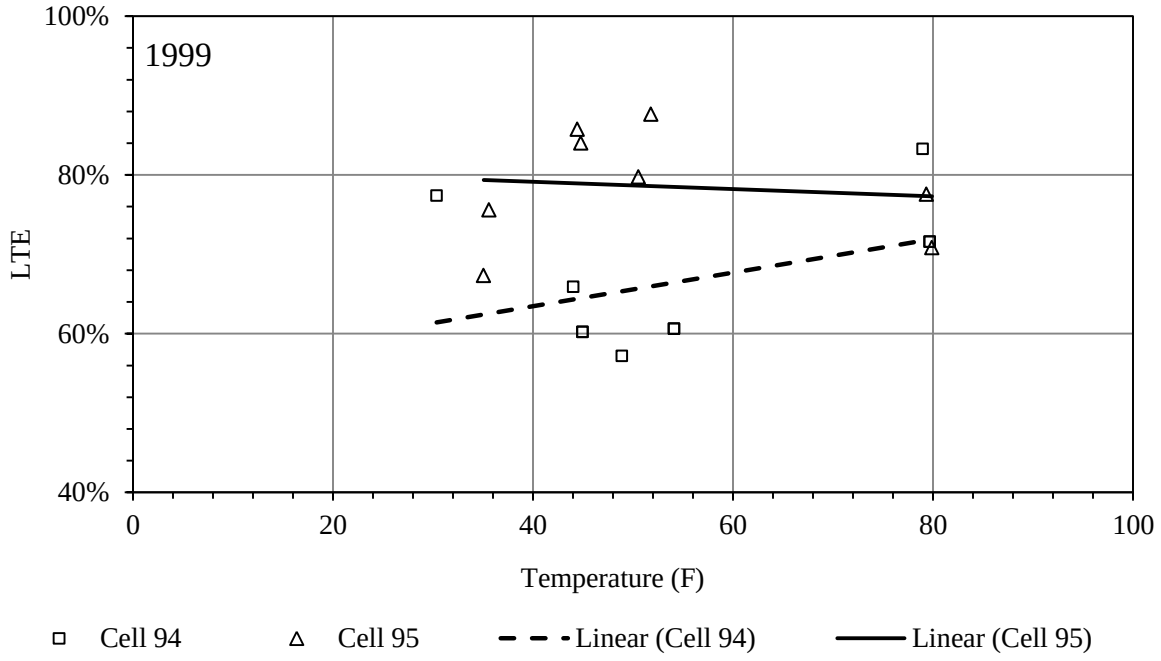

(b)

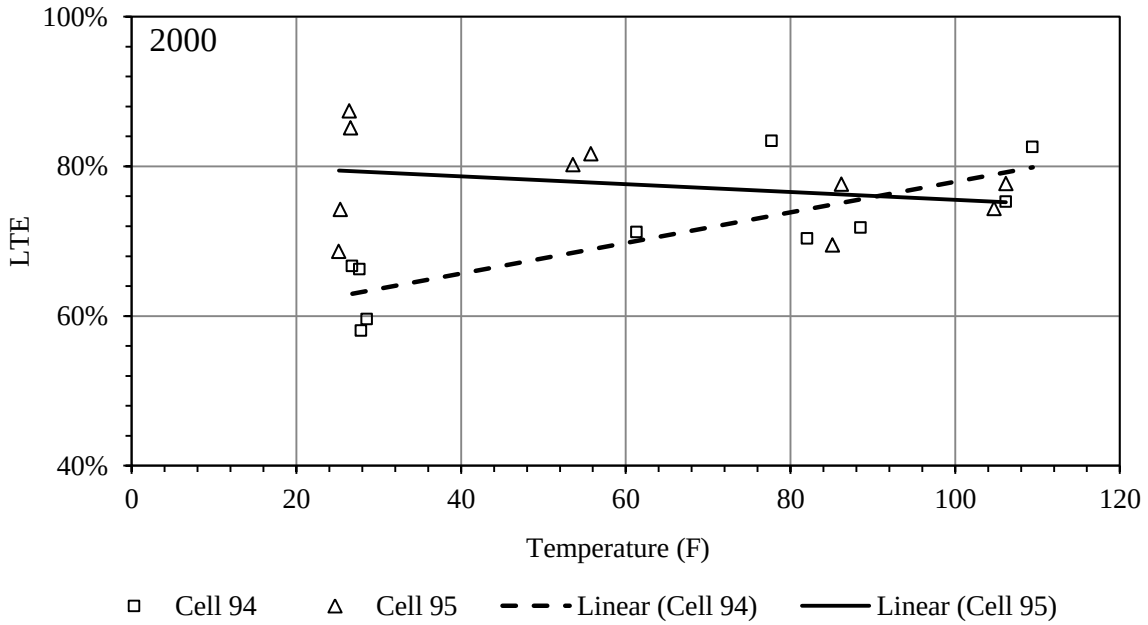

(c)

Figure 2-46: Load transfer efficiency of MnROAD Cells 94 and 95 in (a) 1998, (b) 1999, and (c) 2000.

The studies conducted by Boredelon, 2005 and Roesler, et al., 2008, utilized structural fibers with many shapes such as, straight, twisted and crimped. Both steel and synthetic fibers were

considered. A number of factors that affect the performance of FRC including type, dosage, length, diameter and aspect ratio (AR) of the fibers were considered. AR is the ratio of the length of the fiber to its effective diameter. Table 2-3 presents the features of three different synthetic fibers utilized in the Roesler & Cervantes, 2008 study. The test results for the FRCs with each fiber are also presented in Table 2-3. It can be seen that the peak flexural load and modulus of rupture (MOR) vary with the dosage rate, shape and aspect ratio of the fiber. Dosage rates equal to 4.5 lb/yd^3 in the straight synthetic fiber category and 4.6 lb/yd^3 in the twisted synthetic fiber category seem to provide the highest peak flexural load and MOR. Boredelon, 2005 studied the residual strength ratio (RSR) vs. fiber volume fraction (V_f), as shown in Figure 2-47. The RSR of the FRC is determined by a four point bending test using beam specimens (ASTM-C1609/D1609M, 2010). RSR is expressed as shown below.

$$SR = 100\frac{f_{e,3}}{MOR} \tag{2-14}$$

where $f_{e,3}$ is the residual strength at mid span for a deflection up to (span)/150 of a 24- x 6- x 6-in beam. The span equal to 18 in and therefore the residual strength is measured at 0.12-in deflection.

Bordelon, 2011 also studied the orientation of fibers in the concrete. This study investigated the orientation pattern of a few synthetic fibers with respect to the cast surface of the specimen. Figure 2-49 shows a graph for the structural synthetic fiber, which indicates that the average orientation is around 75 degree from the vertical plane.

Table 2-3: Properties of a few structural synthetic fibers and FRC in the Roesler et al. 2008 study.

Fiber type	Straight synthetic						Twisted synthetic	Crimped synthetic
Cross section	Rectangular						Rectangular	Rectangular
Length (in)	1.57						2.13	2.00
Thickness (in)	0.004						NA	0.03
Width (in)	0.05						NA	0.05
Aspect ratio	90						NA	46
Specific gravity	0.92						0.91	0.91
Volume fraction in the mix (%)	0.19	0.26	0.29	0.33	0.50	0.58	0.30	0.50	0.40
Dosages used (lb/yd^3)	3.00	4.00	4.50	5.00	7.70	8.90	4.60	7.70	6.10
Peak flexural load (lb)	6623	5472	9276	8138	8088	8939	8101	6487	8160
Modulus of rupture (psi)	556	456	773	680	699	745	675	541	673
Testing age (days)	14	14	14	56	56	14	14	14	14

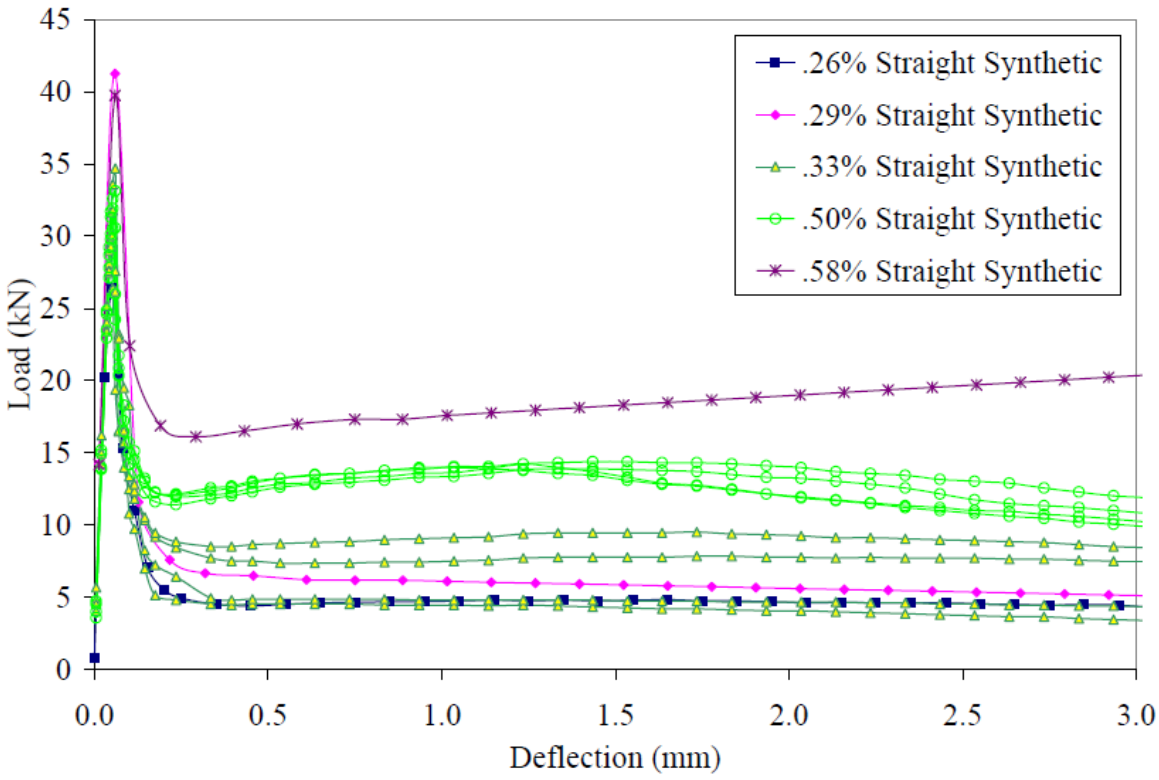

Figure 2-47: RSR vs. fiber volume fraction in Boredelon, 2005 study.

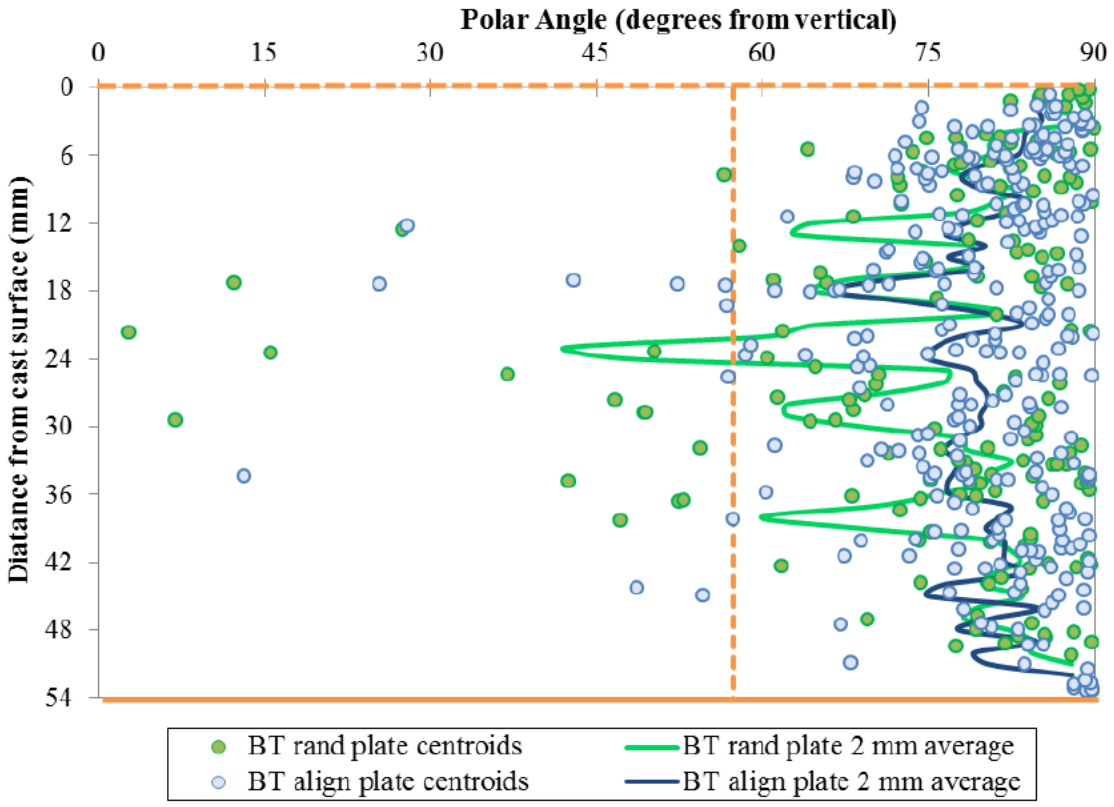

Figure 2-48: Polar angles and average orientation of fibers for each 2 mm with respect to cast surface (Bordelon, 2011).

This current literature about the application of fibers in whitetopping indicates that a substantial amount of research has been carried out to quantify the benefits of different types of fibers in the concrete. Most of this research investigated the benefit of fibers by looking at the change in drying shrinkage, toughness, and modulus of rupture or the residual strength of the concrete. Several experimental and analytical research studies were also carried out to model the crack bridging phenomenon of FRC (Kanda & Li, 1999, Zhang, et al., 2000 and Zhang, et al., 2001). The only study that was found in the literature, which considered the contribution of fibers in joint performance, is by Arnold, et al., 2005, as discussed in Section 2.8. In that work, the peak differential displacement as a function of dosages of hooked end steel fibers was studied. It can be seen in Figure 2-49 that an increase in fiber dosage resulted in a decrease in peak differential displacement. In that study, the failure criteria was established as when the differential displacement reaches 0.06 in. It can be seen that when the fiber was used in the concrete, failure occurs at a wider crack width.

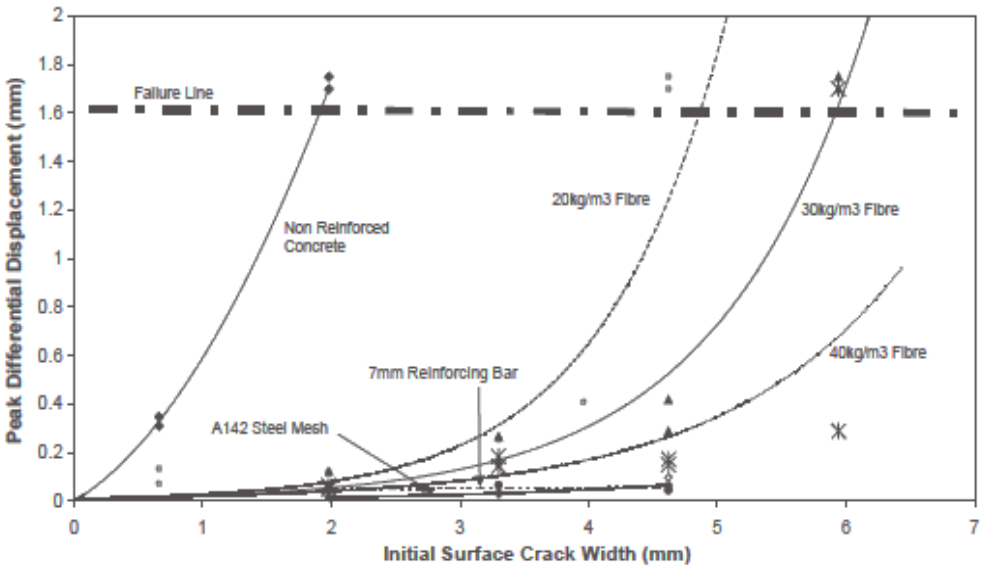

Figure 2-49: Effect of fiber reinforcement in peak differential displacement (Arnold, et al., 2005).

Unfortunately, no significant research has been conducted to characterize the effect of fibers on the load transfer across the cracks and joints. Also only a limited number of research studies investigated the benefits of the application of fibers for bonded whitetopping (Boredelon, 2005; Roesler, et al., 2008; and Rodezno & Kaloush, 2010).

2.11 Conclusion of the Literature Review

This chapter provided an introduction of the whitetopping overlay. The literature survey reveals that the majority of the failures are related to the load induced stress along the wheel path, which is a function of the joint performance. Higher load transfer efficiency is important in order to reduce the debonding of the HMA layer. Lower load transfer between the slabs coupled with the presence of moisture results in distresses in the overlay. Unfortunately, the current design procedures do not consider joint performance criteria. The reason for not considering the joint performance in the design process is because the effect of joint performance on the performance of a UTW has not been well established. The literature review related to the available joint performance evaluation procedures reveals that there is rarely a simplistic procedure that could be adopted to perform laboratory studies for investigating the joint performance of a bonded

whitetopping. Therefore, it is necessary to develop a simple joint performance testing and evaluation procedure. Then it will be helpful to determine whether load transferring materials, such as fiber, can improve the load transfer between the thin slabs. Finally, joint performance shall be incorporated into the design procedure.